

AN ABSTRACT OF THE THESIS OF

WALTER EUGENE EDELMAN, JR. for the Ph. D.

(Name)

(Degree)

in Mechanical Engineering presented on May 8, 1967

(Major)

Title: PHOTOMECHANICS OF STRESS TRANSFER MECHANISMS

IN COMPOSITE MATERIALS.

Redacted for privacy

Abstract approved: _____

Hans J. Dahlke

A study of stress transfer near the ends of the whisker in a simulated whisker reinforced composite material was conducted by using photoelastic techniques. The composite material studied was $\alpha\text{Al}_2\text{O}_3$ whiskers in an aluminum matrix. The photoelastic models used consisted of a scaled-up macroscopic stiffener embedded in a three-dimensional epoxy matrix. The factors controlled during testing were the stiffener geometry, the ratio of modulus of elasticity of the stiffener to that of the matrix, and matrix thickness with respect to the range of influence of the stiffener.

The models were loaded in tension and compression to obtain photoelastic stress patterns. Then these stress patterns were duplicated by locking-in techniques. The models were sliced and analyzed. The normal and shear stress distributions along critical directions and the stress transfer length were determined and compared with the theoretical and experimental results of other investigators.

Copyright by

WALTER EUGENE EDELMAN, JR.

1967

Photomechanics of Stress Transfer Mechanisms
in Composite Materials

by

Walter Eugene Edelman, Jr.

A THESIS

submitted to

Oregon State University

in partial fulfillment of
the requirements for the
degree of

Doctor of Philosophy

June 1967

APPROVED:

Redacted for privacy

Associate Professor Mechanical Engineering
in charge of major

Redacted for privacy

Head of Department of Mechanical and Industrial
Engineering

Redacted for privacy

Dean of Graduate School

Date thesis is presented May 8, 1967

Typed by Marion Palmateer for Walter Eugene Edelman, Jr.

ACKNOWLEDGMENT

On any project such as this there are so many people deserving of gratitude that the acknowledgment could be as long as the thesis itself. It is unfortunate that space prevents naming each individual who participated.

I especially wish to thank my Major Professor, Hans J. Dahlke and his wife Joan for their encouragement. Who among us can ever really describe the bond between the Major Professor and his student? I would also like to thank Wesley Smith, his wife Alice, Charles Heath, and his wife Jessie for their assistance over the years.

There is a group to be singled out for citation: my fellow graduate students. I wonder if it is possible to "go it alone" without the help and encouragement of the other graduate students?

I would also like to thank Jerome C. R. Li. His skills and personal philosophies were a great inspiration and experience.

Last, but certainly not least among those to be named is Jack Kellogg. I wonder how he tolerates all those graduate students breaking drills and dulling cutters? He must be a man of infinite patience.

Finally, I would like to thank the Engineering Experiment Station for their financial support in this project.

TABLE OF CONTENTS

	<u>Page</u>
INTRODUCTION	1
LITERATURE REVIEW	4
THE DESIGN OF THE EXPERIMENT	18
MECHANICS OF CONDUCTING THE EXPERIMENT	25
RESULTS	28
CONCLUSIONS	34
FUTURE WORK	35
HANDBOOK OF STRESS DISTRIBUTIONS	37
BIBLIOGRAPHY	46
APPENDICES	50

LIST OF FIGURES

<u>Figure</u>		<u>Page</u>
1	The model for the law of mixtures.	4
2	The models used in Dow's analysis.	8
3	Tyson's model.	10
4	Schuster's model.	10
5	MacLaughlin's model.	12
6	Shear stress along the matrix-stiffener interface as determined by five different investigators. Square ended stiffener under tensile loading.	30
7	Square ended stiffener, longitudinal distribution of normal stress concentrations in the matrix under the tip of the stiffener and shear stress concentrations along the stiffener-matrix interface.	38
8	Square ended stiffener, radial distribution of shear stress concentrations across the region of the maximum gradient and the region of the widest range of influence.	39
9	Tapered ended stiffener, longitudinal distribution of normal stress concentrations in the matrix under the tip of the stiffener and shear stress concentrations along the stiffener-matrix interface.	40
10	Tapered ended stiffener, radial distribution of shear stress concentrations across the region of the maximum gradient and the region of the widest range of influence.	41
11	18° ended stiffener, tensile loading, longitudinal distribution of normal stress concentrations in the matrix under the tip of the stiffener and shear stress concentrations along each side of the stiffener-matrix interface.	42
12	18° ended stiffener, tensile loading, radial distribution of shear stress concentrations across the region of the maximum gradient and the region of the widest range of influence.	43

<u>Figure</u>		<u>Page</u>
13	18° ended stiffener, compressive loading, longitudinal distribution of normal stress concentrations in the matrix under the tip of the stiffener and shear stress concentrations along each side of the stiffener-matrix interface.	44
14	18° ended stiffener, compressive loading, radial distribution of shear stress concentrations across the region of the maximum gradient and the region of the widest range of influence.	45
15	Typical models used in this investigation.	50
16	Models with square ended stiffeners.	51
17	Models with tapered ended stiffeners.	52
18	Models with 18° ended stiffener.	53

LIST OF TABLES

<u>Table</u>		
1	Tension model, basal parting $\{0001\}$ (square end).	54
2	Compression model, basal parting $\{0001\}$ (square end).	56
3	Tension model (tapered end).	58
4	Compression model (tapered end).	59
5	Tension model, rhombohedral parting $\{10\bar{1}1\}$ (18° end).	60
6	Compression model, rhombohedral parting $\{10\bar{1}1\}$ (18° end).	62

NOMENCLATURE

A_m	Area of the matrix
A_s	Area of the stiffener
d_s	Diameter of the stiffener
E_c	Modulus of elasticity of the composite
E_m	Modulus of elasticity of the matrix
E_s	Modulus of elasticity of the stiffener
G_m	Modulus of rigidity of the matrix
G_s	Modulus of rigidity of the stiffener
k	The stress concentration, either $\frac{\sigma}{\sigma_n}$ or $\frac{\tau}{\sigma_n}$
l	Half-length of the stiffener in Dow's development
L	Applied load
V_o	Volume fraction of stiffeners
x	Generalized distance along a stiffener
ϵ	Generalized strain
ϵ_c	Strain in the composite
ϵ_m	Strain in the stiffener
σ	Generalized normal stress
σ_m	Normal stress in the matrix
σ_n	Normal stress applied to the composite
σ_s	Normal stress in the stiffener
τ	Generalized shear stress

PHOTOMECHANICS OF STRESS TRANSFER MECHANISMS IN COMPOSITE MATERIALS

INTRODUCTION

Technology today is becoming more materials oriented. In fact, there are some members of the technological community who feel that technology is materials limited (9). As a result, technologists today are spending an ever increasing percentage of their manpower and monetary budgets in search of materials to fill specified requirements.

It has long been known that two individual materials can be combined in such a way as to obtain the advantageous qualities of each component. One classical example of a combination of materials are the carbon steels. A small amount of carbon is added to iron to obtain improved properties. In this particular material the carbon is not readily observable in the finished material. In another class of combined materials, the components tend to maintain their individual identities and are visible to the naked eye or under low optical magnification. This class of materials has been given the name "composite materials". Perhaps the best known example of such a composite material of recent times is "fiberglass", the common name for strong glass fibers embedded in a matrix of polyester or epoxy resin.

A new composite material receiving much research attention at this time is the metallurgical whisker reinforced composite. This material is often pictured as being related to fiberglass, but as the technology surrounding whisker composites evolves, theories and mechanisms differing from those in the fiberglass technology are observed (46).

The metallurgical whisker was described by Bell Telephone Company researchers in 1951 and 1952 (3, 14). At that time it was a parasite found to be growing on soldered connections in telephone circuits. These whiskers appeared as tin fibers about two microns in diameter and a few millimeters in length. Due to its small size and the nature of its growth, the whisker approaches being a pure, perfect metallurgical crystal with its attendant high elastic modulus and high tensile strength (4, 17, 19, 29). Studies of whiskers indicate that they grow around a screw dislocation with the direction of the dislocation coincident with the longitudinal axis of the whisker (22). The small size of the whisker reduces the chances of other dislocations or surface defects (19). These factors relate the whisker to the glass fibers used in fiberglass. However, from geometrical considerations, it can be seen that the long length of the glass fiber distinguishes it from the metallurgical whisker.

A look at the chronology of whisker strengthened composite materials (usually called whisker composites) serves as an excellent

introduction to the technology of composite materials (43). The discovery of the whisker was reported in the late 1940's. By the late 1950's the properties of single crystals were being studied by use of whiskers. Then the properties of the whiskers themselves were studied. In the early 1960's a technology for the controlled growth and harvesting of selected whiskers was being developed. At the same time the first feasibility studies concerning the use of whiskers as stiffeners in composite materials were initiated (6, 18). The second half of the 1960's show the first tests of prototype whisker composites. One of the most promising of the whisker composites consists of $\alpha\text{Al}_2\text{O}_3$ (sapphire) whiskers embedded in an aluminum matrix (6, 23, 26). Consequently, this investigation is concerned with this particular system.

LITERATURE REVIEW

Before proceeding further it is necessary to look at past work in composite materials and examine the similarities and differences of the investigations.

Elementary strength of materials develops a "law of mixtures" for monoliths of two materials. The model usually used consists of a bar of material of high elastic modulus embedded in a matrix of lower elastic modulus.

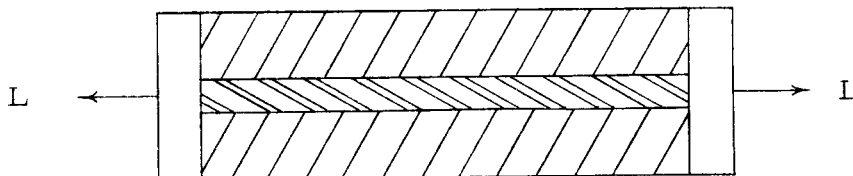


Figure 1. The model for the law of mixtures.

Loads are applied at the ends. It is assumed that the end effects are negligible and that all portions of the monolith are strained equally. Since the strains on both sides of the stiffener-matrix interface are the same, there is no shear stress along the interface. The ratio of stresses carried by the stiffener and the matrix can be computed from the equality of the strains.

$$\epsilon = \frac{\sigma_s}{E_s} = \frac{\sigma_m}{E_m}$$

or

$$\frac{\sigma_s}{\sigma_m} = \frac{E_s}{E_m}$$

The load carried by the monolith is then a function of the stresses in the stiffener and the matrix and of their respective areas.

$$L = \sigma_s A_s + \sigma_m A_m$$

The load carrying capacity and the average elastic modulus of the monolith can be computed from the previous relationships.

$$\sigma_c = \frac{L}{A_c} = \frac{L}{A_s + A_m} = \frac{\sigma_s A_s + \sigma_m A_m}{A_s + A_m}$$

$$\sigma_c = E_c \epsilon_c = \frac{\sigma_s A_s + \sigma_m A_m}{A_s + A_m} = \frac{E_s \epsilon_s A_s + E_m \epsilon_m A_m}{A_s + A_m}$$

since

$$\epsilon_c = \epsilon_s = \epsilon_m$$

$$E_c = \frac{E_s A_s + E_m A_m}{A_s + A_m}$$

Now, assume that the areas of the stiffeners are some fraction V_0 of the total cross sectional area. By the model sketched in Figure 1, the volume of the stiffener will be the same fraction V_0 of the

volume of the monolith.

So,

$$E_c = \frac{E_s V_o A_c + E_m (1 - V_o) A_c}{A_c}$$

or

$$E_c = V_o E_s + (1 - V_o) E_m$$

This is one of the forms of the law of mixtures. The model used in the development assumed uniform strain, a consistent geometry of the stiffener and the matrix, and perfectly elastic properties.

The theoretical technology concerning fiberglass reinforced plastics often uses a different model due to properties of the materials involved and the nature of fabrication. When the fiberglass reinforced plastic consists of parallel strands of glass embedded in the matrix, the previous model is still suitable. However, if the fibers are not parallel, as is the case in continuous glass strands wrapped in alternating layers around objects or in the case of glass matting, the previous model does not hold. In this case it is often appropriate to consider the glass fibers to be much stronger and have more volume than the matrix. Hence, all of the load is assumed to be carried by the glass fibers. The fibers are assumed to form a net and the term netting analysis is applied to the study of the strength of this model (32).

It is apparent that the rather low aspect ratio¹ of the metallurgical whisker is a serious handicap in applying the fiberglass models. Netting analysis is rejected per se since a matrix is necessary to transfer the loads between the relatively short whiskers (27). The law of mixtures from elementary strength of materials may appear to be too simple because of the assumption that stiffeners are aligned parallel to the load. However, recent developments in manufacturing technology have produced whisker composites with axially aligned whiskers, so this may not be as serious a handicap as might be expected. The whiskers can be aligned in critical directions as necessary (2, 17, 23, 26).

There have been several analytical approaches to the problem of stress transfer mechanisms in the whisker composite (5, 10, 15, p. 45-47, 20, 38, 40, 41, 47 Chap. 2). Dow's theory is quoted more often than all the others, partly because it was developed specifically for whisker composite and partly because it contains tables for engineering materials (10). He uses the model of a cylindrical whisker embedded with a cylinder of matrix material (Figure 2). Due to symmetry this model is cut at the half length and considered

¹The ratio of the stiffener length to diameter is called the aspect ratio. In a short stiffener such as a whisker, any ineffective part of the stiffener that is not fully loaded appears as a reduction of the aspect ratio and consequently reduces the theoretical strengthening qualities of the stiffener.

fixed at that position. A tensile load is applied either to the stiffener or to the matrix.

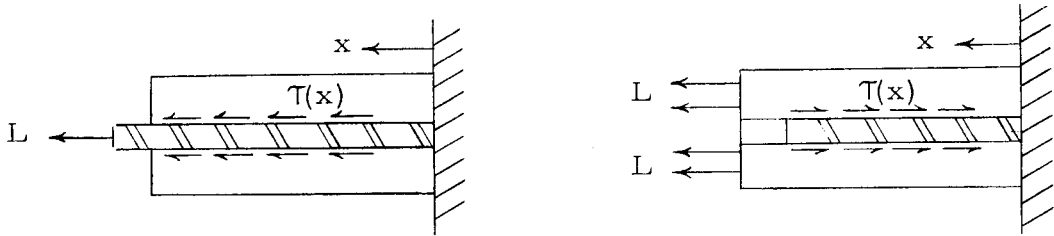


Figure 2. The models used in Dow's analysis.

Dow's solutions for the shear stress distribution $\tau(x)$ along the stiffener at the interface take the same form for either method of loading.

$$\tau(x) = \frac{\lambda}{4} \left[\frac{L}{A_m \left(\frac{E_m}{E_s} \right) + A_s} \right] \left[\frac{\sinh\left(\lambda \frac{x}{d_s}\right)}{\cosh\left(\lambda \frac{l}{d_s}\right)} \right]$$

The parameter λ is given by

$$\lambda = 2 \sqrt{\frac{2\sqrt{2} \left(\frac{G_s}{E_s} \right) \left[1 + \frac{A_s}{A_m} \left(\frac{E_s}{E_m} \right) \right]}{(\sqrt{2} - 1) + \left(\frac{G_s}{G_m} \right) \left[\sqrt{\frac{A_m}{A_s}} + 2 - \sqrt{2} \right]}}$$

It should be noted that the models and their assumptions avoid the problems of any singularities near the corners. They also neglect any

load carrying capacity and singularities at the end of the stiffener. A satisfactory value for the modulus of rigidity (G_s) appearing in the expression for the parameter λ has not yet been determined for an $\alpha\text{Al}_2\text{O}_3$ whisker. In his development of charts for use with real materials, Dow assumed the ratio of $G/E = .385$ for all materials. In the discussion of his results he has noted these difficulties, particularly singularities near the corners and at the end of the stiffener.

Experimental developments in composite materials can be grouped according to the background of the investigator. Basically they involve the microscopic techniques of the metallurgist or the macroscopic techniques of the photoelastician (6, 27).

The metallurgical approach consists of embedding stiffeners in a matrix and then loading in tension until failure occurs. The nature of the failure is analyzed by metallurgical techniques of polishing and etching. Thus far, the model materials have consisted of both whiskers embedded in a matrix and fine wires embedded in a matrix (17, 18, 24, 36, 37, 39).

Photoelasticians have made up macroscopic two-dimensional models with a strong metal stiffener embedded in a matrix of birefringent photoelastic material. Tyson, in his experiment, milled a slot in a sheet of photoelastic material and fitted a square ended aluminum stiffener to the slot and glued it in place (45). The loads were applied through the matrix in such a way as to represent a

semi-infinite stiffener quite similar to the model proposed by Dow, but limited to two dimensions for ease of photoelastic analysis (Figure 3).

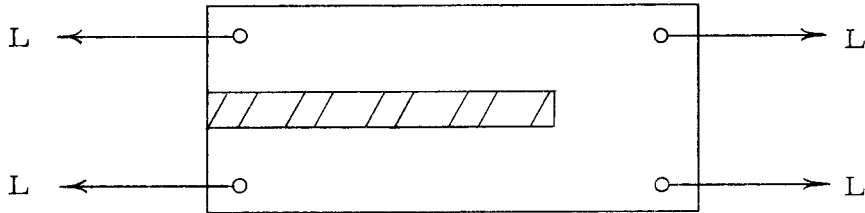


Figure 3. Tyson's model.

Schuster, in his experimental work, embedded $\alpha\text{-Al}_2\text{O}_3$ whiskers in a matrix of photoelastic epoxy (42). The model was cut to the "dogbone" shape used in standard test work. The whisker was located in the narrow or active area of the specimen. Tensile loads were applied through the matrix at the ends of the specimen (Figure 4).

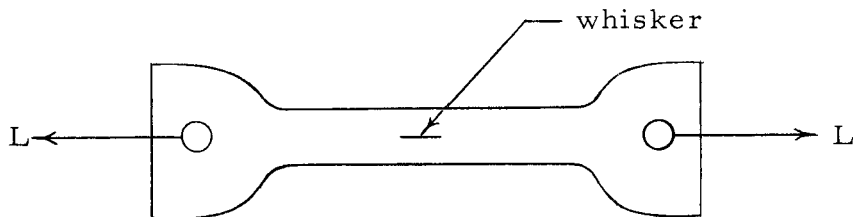


Figure 4. Schuster's model.

Since the specimen used a three-dimensional matrix surrounding the whisker, the standard two-dimensional photoelastic analysis did not apply. Due to the small sizes involved it was impractical to use the slicing technique of three-dimensional photoelasticity. In order to obtain a suitable method of data reduction for the small model he assumed that a localized stress concentration near the whisker would cause a radial stress distribution. He further assumed that this distribution would be linear and integrated the photoelastic effect of the radial stress distribution through the visible range of influence. This provided an analytical relationship between the localized stress condition and the observed photoelastic condition. By reversing the process he could correct his observed photoelastic data to obtain the localized stress condition at the surface of the whisker.

MacLaughlin used a macroscopic two-dimensional photoelastic analysis similar to that of Tyson (25). His models consisted of steel stiffeners of various end shapes. These were embedded in a two-dimensional matrix² of photoelastic epoxy. About three diameters away from the stiffener a U shaped frame surrounded the epoxy matrix. Tensile loads were applied to the stiffener and the U shaped frame (Figure 5).

²A two-dimensional matrix means that the matrix is the same thickness as the stiffener and does not fully encompass the stiffener.

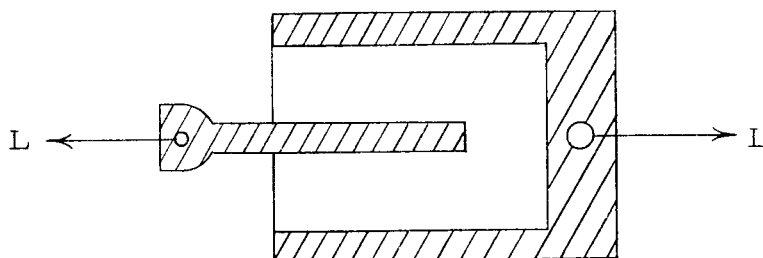


Figure 5. MacLaughlin's model.

In order to test for the effects of load carrying capacity across the end of square ended stiffeners, he cast some models with the end surface coated with wax to provide a deliberate unbond. His analysis was a conventional two-dimensional photoelastic analysis and the shear stresses along the boundaries of the stiffeners are given.

At this point the author would like to combine the preceding investigations to point up some of the motivations for this project.

Virtually every publication on the topic of composite materials includes the "law of mixtures" in some form. Usually this law is modified by assuming an ineffective length of the stiffener, near the ends, where stresses are not uniform along the boundary of the stiffener. This ineffective length for stiffeners has not been determined, and at this time it appears it may have to be determined on an ad hoc basis for each selection of stiffener and matrix. Dow's

theory gives a picture of the order of magnitude of the ineffective length. As he points out however, the shape of the end of the stiffener has been considered as flat and incapable of carrying a load. If these variables are included, the stress distributions near the end of the stiffener are altered and the stress concentrations at or near singularities may limit the usable strength of the composite. Dow has predicted that a great increase in strength will be achieved by using a ductile matrix and allowing the matrix to deform plastically around the ends of the stiffener. This will cause a localized region of work-hardened matrix at points of critical stress concentrations. The appendix of Dow's report includes an approximation to this situation for an aluminum matrix by approximating the true stress-strain curve with a series of straight lines. However, it still avoids the problem of the end conditions by using the models shown in Figure 2.

The experiments performed by the metallurgical techniques of loading a tensile specimen to failure and then subjecting a prepared portion of the failed region to microscopic analysis support Dow's predictions of localized plastic flow around the ends of the stiffeners (17, 19, 20, 39). In the case of materials made from fine wires embedded in a matrix, the wires also showed yielding in the sense of a necked-down section (18, 21). This would not be appropriate to the situation with whiskers as stiffeners because a whisker is a single crystal and will not neck-down. The whisker will elongate

approximately five percent before failure occurs, however.

The photoelastic studies have generally been in agreement with Dow's development. However, the investigators themselves have continuously questioned whether their photoelastic models were representative of the prototype material. Tyson's two-dimensional model was fabricated by machining, and the square-ended, aluminum stiffener was glued into the matrix. The matrix was a photoelastic material with a modulus of elasticity of 470,000 psi. The ratio of elastic moduli of stiffener to matrix for these two materials is slightly over 20:1, where the prototype material, $\alpha\text{Al}_2\text{O}_3$ in aluminum would have a ratio of 6:1. The width of the matrix surrounding the stiffener is four fiber diameters on each side. There is some question that this is adequate to avoid edge effects.

Schuster's work used one component of the prototype material, $\alpha\text{Al}_2\text{O}_3$ whiskers, in the photoelastic model. The modulus of elasticity of 430,000 psi for the photoelastic material used was rather low as compared to that of aluminum, the prototype matrix. As a result the moduli ratio between the stiffener and the matrix is about 150:1. The amount of matrix surrounding the stiffener was observed to extend beyond the visible range of influence so there should be no edge effects. The very small physical size of the whisker embedded in the photoelastic matrix prohibited using the customary three-dimensional analysis technique of locking in the stress patterns and

slicing the model into sections. Schuster solved this problem by assuming that the radial stress distributions were linear and their effects could be integrated throughout the visible range of the photoelastic model. This novel approach to the problem has not been verified by other investigators and physical size may prevent its being verified by conventional techniques.

MacLaughlin's work is the most comprehensive from the standpoint of controlled geometry of the stiffener. His two-dimensional models have a wide variety of end shapes and include deliberate unbonds in the case of square ends. In his experiment the stiffeners were made of steel and the matrix was a very soft photoelastic material. The ratio of elastic moduli was 3000:1. The method of loading consisted of pulling on a U shaped frame surrounding the matrix of the model. The distance from the stiffener to the frame was about three diameters. Hence, there may be interaction effects between the stiffener and the loading frame. It is interesting that this is the first question that MacLaughlin raises in his discussion. He also questioned the ratio of elastic moduli and the effects of limiting the models to two dimensions.

From the foregoing discussion it can be seen that certain aspects of the scaled up photoelastic model can be improved. The problem of finding the correct scaling factors is twofold. First, very little is known about the whisker. Its geometry and modulus of

elasticity have been determined. By its crystallographic structure it should not have a unique value for Poisson's ratio, but some approximations have been made. Virtually nothing is known about surface conditions that manifest themselves at the interface when the whisker is embedded in a matrix (23, 31). The only real "knowns" about whiskers are the geometry, the modulus of elasticity in tension, and their price (28, 46). The latter does not enter into this investigation.

The second part of the scaling problem involves locating materials with correct parameters for a scaled experiment. This in itself can be a major undertaking. In this investigation it was possible to control certain parameters for purposes of a scaled experiment. The first was the geometry. Schuster indicated that his model was larger than the "range of influence" of the stiffener, and he does give some information as to the range of influence. The geometry of the stiffener should match that of the prototype stiffener, $\alpha\text{Al}_2\text{O}_3$, in this case.

The ratio of elastic moduli has always been questioned. This should be controlled by selection of materials.

The use of two-dimensional models to simulate a three-dimensional situation has been questioned. It would be appropriate to use three-dimensional models, but use the more customary slicing method of photoelastic analysis of three-dimensional models

rather than Schuster's integration technique.

The photoelastic models should be assembled in a manner that approximates the prototype material, with particular attention paid to the contact between the stiffener and the matrix at the interface.

The loading should be controlled to verify that compressive behavior is the same as that for tensile loading.

Finally, in the analysis and reduction of data there are three regions near the tip of the stiffener that may have critical stress concentrations, but previous work has not indicated the magnitudes of these concentrations. The normal stress directly under the tip of the stiffener may be a region of incipient material failure and should be included in the analysis. There is a region near the tip that has a very steep shear stress gradient which could lead to crack propagation. This should be investigated. There is also a point a few diameters in from the tip where the stiffener shows its greatest radial range of influence. Although this is not a critical region for incipient failure, some knowledge of the stress distribution in this region would be helpful in determining interactions between adjacent stiffeners.

THE DESIGN OF THE EXPERIMENT

Before going into the details of this investigation it is appropriate to outline the design of the experiment. The first stage consisted of developing a three-dimensional photoelastic model that appropriately controlled the stiffener geometry, the matrix to stiffener geometry, the ratio of elastic moduli between stiffener and matrix, and the process of manufacture. The models were then subjected to tensile and compressive loads. The resulting photoelastic fringe patterns caused by these loads were observed. Next, these fringe patterns were duplicated and locked into the models by "locking in"³ techniques. A slice was removed from the center portion of the model in such a way as to give a two-dimensional picture of the stresses surrounding the stiffener. This slice was then analyzed by the usual two-dimensional techniques of photoelasticity (12, Chap. 8). Symmetry conditions allow the slice to be representative of any of the planes passed through the stiffener in a manner such that the stiffener lies in the plane of analysis (30).

³The term "locking in" is used to describe the process of permanently establishing photoelastic patterns in a birefringent material. This procedure is often called "stress freezing", but the latter term is a misnomer since the stresses themselves are not frozen in, but only a photoelastic pattern similar to that generated by stress is frozen into the material. The term "locking in" more correctly describes the phenomenon and will be used in this investigation.

The instrument used for the photoelastic analysis more or less determined the maximum size of the photoelastic model. The one inch field of the Photolastic type 052 polariscope and its associated loading frame appeared to limit the size of the models to one inch by one inch by fourteen inches. The photoelastic model was to be compatible with the model selected by Dow except that it would provide for various end shapes and loadings. Thus, the outside diameter of the cylinder of the matrix was limited to one inch. The model was to be of the semi-infinite type as shown in Figure 2. Loads were applied to end plates cemented to the model at positions away from the range of influence of the stiffener. The matrix material was selected from several photoelastic epoxy systems. CIBA type 502 resin with 20 pph of CIBA type 956 hardener was used for all models. This particular system was selected for its room temperature curing properties, an exothermic reaction that could be controlled with standard laboratory equipment, low absolute shrinkage during curing, and its suitability for locking in techniques. The modulus of elasticity of this material in the fully cured state is 382,000 psi. The modulus of elasticity and the photoelastic fringe coefficient were linear to at least 5400 psi. Since the modulus of elasticity of the matrix is determined by the epoxy system used, the selection of the material for the stiffener has to be based on the desired ratio of elastic moduli. Yellow birch dowel was used for the model of the

stiffener. By selecting the dowel for straight and uniform grain, samples were obtained with a fairly uniform tensile modulus of elasticity of 1.97×10^6 psi. The ultimate tensile strength was 19,000 psi, so failure should occur in the matrix rather than the stiffener. The ratio of elastic moduli between these two materials is about 5:1 whereas the prototype material has a ratio of 6:1.

The geometry of the stiffener was determined by the method of growing and harvesting $\alpha\text{Al}_2\text{O}_3$ whiskers and from crystallographic data. The whiskers are grown by vapor condensation and the finished product appears as a cluster of acicular needles rising out of the boat that serves as the base during the growth phase (22). The whiskers are harvested by breaking the fixed end near the boat. Thus, the free end appears as a needle shape and the harvested end is a broken end. From crystallographic data, it has been determined that $\alpha\text{Al}_2\text{O}_3$ can part across either the basal $\{0001\}$ or the rhombohedral $\{10\bar{1}1\}$ plane (7, p. 70, 188). This gives two possible planes, one perpendicular to the longitudinal axis and one that cuts the longitudinal axis at an 18° incline. The angle of the free or needle shaped end is not so well known. A sample of selected $\alpha\text{Al}_2\text{O}_3$ whiskers was examined and it was determined that the included angle of the needle shaped end varied from 5° to 6° . These three end shapes, the needle, the square, and the 18° , comprised the models studied. The cross section of the $\alpha\text{Al}_2\text{O}_3$ whisker is hexagonal. It was felt that no

observable error would occur if a circular cross section were used in the scaled up stiffener. The surface of an $\alpha\text{Al}_2\text{O}_3$ whisker is "smooth" as compared to a whisker of SiC, but smoothness is a relative term and adequate standards have not been set up to provide a measurable description of surface smoothness (1, 2). One approach was tried, however. Since the surface of wood is quite porous, it was felt that the pores may provide an unrealistic situation for mechanical adhesion by allowing tendrils of epoxy to penetrate into the pores (11, Chap. 2). Consequently, several surface finishes that would more or less duplicate the mechanical porosity of $\alpha\text{Al}_2\text{O}_3$ were tried. One indication of the surface effect is a wetting test. A wetting test of the selected epoxy on a large single crystal of sapphire (Al_2O_3) was conducted according to ASTM D-724. A polyurethane varnish applied to the dowel was found to best duplicate the wetting characteristics of the sapphire crystal. This completed the geometry phase of scaling up the whisker.

Selecting the geometry between the stiffener and the matrix was done by trial and error involving several models. As it was noted earlier, the photoelastic model was to be compatible with Dow's model except that it should make provision for various end shapes and loadings. For manufacturing ease the models have square rather than cylindrical cross sections. The range of influence of the stiffener had to be determined so that a satisfactory ratio

of matrix to stiffener area could be selected. Theoretically, the range of influence of the stiffener extends infinitely in any direction, but its practical limit is placed where the photoelastic effect is no longer observable. Due to the maximum one inch by one inch size of the model, the size of the stiffener was varied until it was small enough. The procedure was similar to that used in the final analysis. The model was loaded and the stress pattern was observed. Then this pattern was duplicated by locking in techniques. Finally, by taking the center slice out of the model, it was possible to determine if there was visible influence of the fiber at the boundaries of the slice. A maximum range of radial influence of six stiffener diameters was observed. Consequently, dowel with a minimal diameter of 0.080 inch was selected.

The problem of duplicating fabrication techniques is a major project in itself. Little is known about residual stresses occurring in the prototype material (8, 13, 15, p. 166, 33, 34). Experiences in this project showed that in the production of photoelastic models, residual stresses could be produced that were large enough to destroy the model before any loads were applied. It was decided that this investigation would be limited to stresses produced by external loads. Consequently, the photoelastic models were produced to be free of residual stress patterns. The technique of casting the photoelastic matrix around the stiffener better approximated the

fabrication of the prototype material than the gluing of the stiffener into the matrix since it provided a more intimate contact at the interface and tended to eliminate glue line problems.

After an adequate cure time the models were ready for loading. End plates were glued on to distribute the load and for ease of loading. The stress patterns under load were observed from no load up to the point of apparent failure. It was noted that the geometry of the patterns was repetitive with only the number of fringes changing with load. This would indicate that within the load region below the failure point, any load is representative of all loads. A test for this will be described later.

The next step was to duplicate the stress patterns generated by loading and lock them in with the locking in techniques. This was accomplished by heating the model to about 60°C and applying a light load. The stress pattern then gradually crept in and was more easily controlled than was the case when a higher temperature was used. It should be noted here that there was some concern about the difference in geometry of the stress patterns near the edges of the locked in patterns as compared to those generated by loading. Some development work led to a better duplication of the load generated patterns. The cooling rate at the outside surface was increased and the edge fringes changed their directions to match those obtained under loading. Slices taken from development models indicated that

this is probably a minor effect and is observed only because the effect is integrated throughout the entire thickness of the model whereas the concentrated stresses at the tip of the stiffener are localized and are integrated through only a small portion of the model.

After the stress patterns were locked in and the model was cooled to room temperature, a slice 0.10 inch thick was taken from the center of the model. This slice, containing the stiffener, was analyzed by conventional two-dimensional photoelastic techniques. The slice was taken by conventional techniques; a rough cut was made on a band saw and then milled to yield smooth and parallel surfaces. It was found that a coating of silicone oil on the surface gave satisfactory optical results, so polishing the surface was not attempted.

MECHANICS OF CONDUCTING THE EXPERIMENT

The photoelastic models prepared as described in the previous section were loaded along the longitudinal axis to establish the stress at failure and to observe the stress patterns generated. It was observed that the stress pattern was repetitive; that is, the photoelastic fringes had the same general shape, but the number varied linearly with load. In order to verify this observation with respect to two-dimensional conditions the following experiment was conducted. Five models of the square ended configuration were loaded in compression and the stress patterns were locked in. The loads were selected so that the loading range from zero to failure was covered in five approximately equal steps. After locking in the stress pattern, the models were sliced and the center section removed for analysis. It was observed that the two-dimensional stress patterns were geometrically similar. The isoclinic patterns were also similar. However, in the highly stressed models the isoclinic patterns were harder to resolve due to interference with the stress fringes. One of the underlying foundations of this investigation is that the analysis performed on a two-dimensional slice accurately represents the situation occurring in the three-dimensional model. Since it was determined earlier that in the three-dimensional case the number of fringes varied linearly with load, it was now necessary

to determine that the number of fringes in the two-dimensional slice vary linearly with the number of fringes in the three-dimensional model. The regression of the number of two-dimensional fringes on the number of three-dimensional fringes was observed to be linear. This then implies that any one model is representative of all models and the stresses at critical points can be described in terms of stress concentration factors.

As it was pointed out above, the isoclinic patterns were increasingly difficult to resolve as the number of stress fringes increased. This has been observed by other investigators in photoelasticity and the usual technique is to decrease the load to improve the resolution of isoclinics. Decreasing the load will reduce the number of stress fringes and make their resolution somewhat less accurate. A compromise selection of a stress pattern of about 30 percent of the failure load was found to yield good results in resolving both the stress fringes and the isoclinics. All further tests were conducted to approximate this load.

For the final experiment in this investigation the stress patterns simulating tensile and compressive loads for each of the three end geometries were locked into the models. A center slice 0.10 inch thick was taken from each model. The normal stresses along the longitudinal axis were determined by the shear difference method. The shear stresses along the stiffener, across the region

of the steepest stress gradient, and across the widest transverse range of influence were also determined. These stresses were normalized to stress concentration values by dividing by the value of stress observed in a portion of the matrix away from the range of influence of the stiffener. The results appear in Figures 7 through 14 in the Handbook Section.

RESULTS

The first and most significant result of this investigation is the difference in stress distributions between tensile and compressive loadings. The compressive stress concentrations are higher than those in tension and their influence is observable a greater distance away from the stiffener. The reason for this is not clear at this time. One plausible explanation is that the high numerical values of stress concentrations have led to incipient failures in adhesion. The tensile model requires better adhesion than the compressive model since the compression loads can be transmitted by direct bearing stresses. The models used in this experiment were examined carefully for any adhesion failures and none were observed either macroscopically or microscopically. Because the situation at the interface is vague in all composite materials, additional tests were conducted using different surface coatings, but the results substantiated previous findings. It was felt that the laminated nature of the birch stiffener may have been at fault, but the same general differences in stress patterns were observed when using steel and aluminum stiffeners. Finally, it was felt that the semi-infinite model may not have been representative in its loading method so models with fully enclosed stiffeners were constructed and tested. Again, these substantiated the previous findings. Perhaps the most likely place to

look for an explanation is in the interface phenomena since this seems to be the region of greatest lack of knowledge in composite materials technology.

The second significant result is that stress concentrations appear to be highest in the case of the square ended stiffener and least in the case of the tapered end. This is in agreement with findings of other investigators (23, 42). From a numerical standpoint there is only one configuration where a fairly direct comparison can be made: the case of the square ended stiffener under a tensile load. Tyson's work indicates that the maximum shear stress concentration along the stiffener was about 3.8:1. MacLaughlin obtained a value of 3:1; Schuster, 2.5:1; and this investigator, 2.17:1. Dow's theory predicts a maximum concentration of 1.7:1 for this investigator's configuration. It should be repeated that these are maximum values and they do not occur at the same location in each experiment. A better comparison of the results of each investigator can be made by examining the shear stress distributions along the stiffener (Figure 6). When observed in this manner it is readily seen that each of the photoelasticians obtained a higher maximum stress concentration than that predicted by Dow. This may well be due to the simplified end conditions used in Dow's theory. Also, in the photoelastic work, the two-dimensional models showed higher stress concentrations than the three-dimensional models. Even more important than the

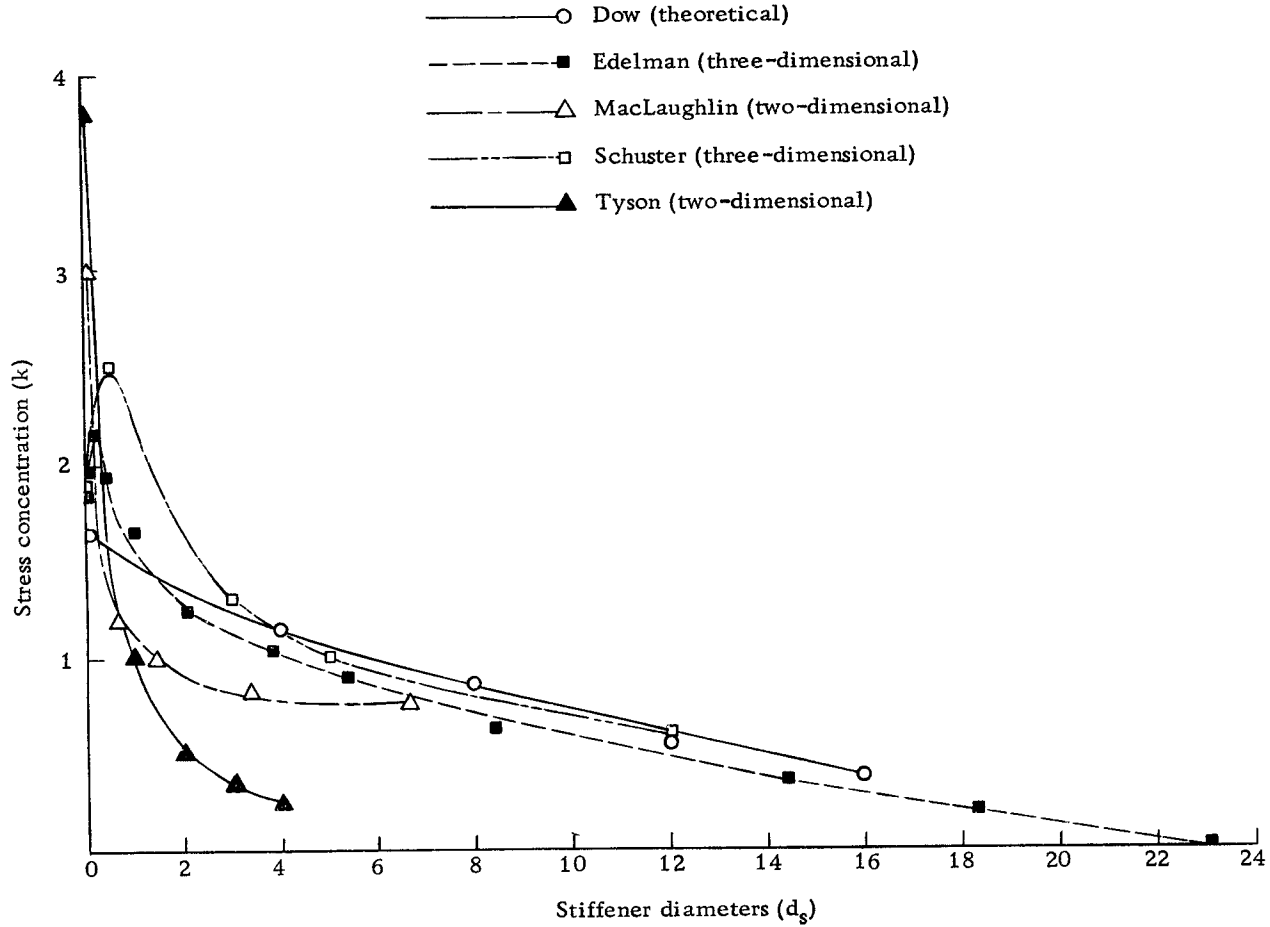


Figure 6. Shear stress along the matrix-stiffener interface as determined by five different investigators. Square ended stiffener under tensile loading.

comparison of maximum values of stress concentrations is the shape of the stress distributions. The stress concentrations in the two-dimensional models decrease very rapidly with increasing distance from the end of the stiffener while in the three-dimensional models the stress concentrations rise slightly and then decrease at a slower rate. At distances greater than five diameters from the end, the three-dimensional distributions are in better agreement with the theoretical prediction. A similar conflict in the shape of stress distributions was observed in the tapered ended stiffener when MacLaughlin's two-dimensional model was compared with the three-dimensional model of this investigator. When considering these results it should be remembered that each investigator changed more than one treatment used by the other investigators. Tyson and MacLaughlin used two-dimensional models. Schuster and this investigator used three-dimensional models. The ratios of elastic moduli ranged from 3000:1 in MacLaughlin's experiment, 150:1 in Schuster's, 20:1 in Tyson's, and down to 5:1 in this experiment. MacLaughlin used a different type of loading frame from those used by the other investigators and Schuster used a novel method of data reduction. In view of all these differences it is surprising that the results show such close agreement.

Third, the ineffective length or transfer length is relatively short with the stiffener carrying the full load within 25 to 30

diameters from the endpoint. This is in agreement with the theoretical developments of Dow. For the values of elastic moduli and areas selected for models used in this investigation Dow predicted a minimum ineffective length of 20 diameters. Due to the nature of his mathematical model, the maximum ineffective length approaches infinity. However, in order to put a practical value on the upper bound, full stiffening was said to be achieved when the shear stress between the stiffener and the matrix fell to the minimum value detectable by the photoelastic methods used in this investigation. Under these conditions Dow's theory predicts an ineffective length of 38 diameters. The manner in which the measured values fall toward the low side of this range may be indicative of the amount of reinforcement provided by the load carried across the end of the stiffener. The measured ineffective lengths would decrease if the matrix were allowed to yield and provide additional stiffening by localized work hardening.

Fourth, in the matrix, the range of influence of the stiffener drops off quite rapidly and falls to zero in the order of five or six diameters. This furnishes some information for use in determining the volume fraction of stiffeners necessary to provide adequate stiffening in the prototype material (23). For example, if a composite were to be designed such that each stiffener acted independently, the volume fraction (V_0) would have to be less than two percent.

Presently such a volume fraction is being investigated for use in dental work.

Fifth, it was observed that two different types of failure took place and the type observed depended on whether the loading was tensile or compressive. With tensile loading the initial failure started with a shear crack at the tip of the stiffener. In the case of the square ended stiffener the crack continued across the end to the corner and then continued into the matrix along the direction of the steepest stress gradient. In the case of the 18° and tapered ends the crack also continued into the matrix along the direction of the steepest stress gradient. Failures under compressive loads were analogous to those of the rigid punch penetrating a yielding material. There was an obvious failure in shear along the sides of the stiffener in the manner predicted by Outwater (32). There may have been a failure directly at the tip, but the nature of the compressive loading allows the continued transfer of stresses by direct compression bearing. The dependence of the two methods of failure on the direction of loading may be linked to the differences in stress distribution with direction of loading. There is certainly some room for more work in this area.

CONCLUSIONS

In the composite material studied, the behavior of the stresses in the region surrounding the tip of the stiffener depends on the direction of loading and the geometry of the end shape. The numerical values of these stresses at various stations appear in Figures 7 through 14 in the Handbook Section.

The differences in stress distributions obtained in the case where experiments of several investigators were compared indicated that the three-dimensional photoelastic technique provided a better model than the two-dimensional technique.

The mechanism of failure observed varied with the direction of loading. The failure was along the stiffener for compressive loading and at 90° to the stiffener for tensile loading.

FUTURE WORK

This investigation represents an examination of a minute part of a particular composite material. Only the stress transfer near the tip of the stiffener has been considered and the loading was such as to keep both materials in the elastic region. The question as to whether this truly represents the situation in the prototype material may well be asked. The matrix used in this investigation was a photoelastic epoxy, which tends to be brittle and has no plastic region. In the prototype composite material the matrix is ductile and has a plastic region. Thus, there may be some additional strengthening due to localized yielding and work hardening. A great deal could be learned if a photoelastic material with a reasonable plastic region were used. Photoelasticians are working on such materials at this time. The question then arises about the comparison between the birch stiffener used and the prototype stiffener $\alpha\text{Al}_2\text{O}_3$. Very little is known about the elastic properties of the prototype stiffener, so modeling is a rather difficult procedure due to lack of data about the prototype as well as finding a modeling material with the right characteristics. Also, little or nothing is known about the adhesion and wetting characteristics at the interface (23, 31, 35, p. 74, 39 44). Many of the manufacturing processes would lead to problems such as residual stresses, and these would manifest themselves in

this region. All of these difficulties should be investigated in detail. However, the limits of time and money do not permit such an idealistic approach. The author feels the most pressing problems that can be reasonably investigated at the present concern the differences between tensile and compressive loading, residual stresses due to manufacturing processes, and elastic instability. The latter was not dealt with at all in this investigation.

If the difference between tensile and compressive loading turns out to be an interface phenomenon, it may not be possible to pursue the topic further until more data on the interface become available.

The problems of residual stresses and elastic instability will probably be easier to approach because much of the groundwork has been laid in terms of modeling and scaling factors.

From an analytical standpoint, it is necessary that the mathematical model be refined to include variations in stiffener shape, loads at the end of the stiffener, and direction of loading. It is hoped that the results of this experiment will provide some insight into the nature of the analytical solution.

HANDBOOK OF STRESS DISTRIBUTIONS

Figures 7 through 14 constitute a handbook of stress distributions for the various model configurations studied in this investigation. In order to present as much comparative information as possible, several graphs have been combined to make each figure. A scaled drawing of the stiffener appears in each figure. The stress distributions along certain critical directions are shown in their relative positions with respect to the stiffener. The stress concentrations are denoted as k and the relative location is given in dimensionless units of stiffener diameters d_s . In the case of the two symmetrical models, both the tensile and compressive loadings are shown in the same figure. Since the stress distributions were not symmetrical in the case of the 18° ended stiffener, the results for tensile loading and compressive loading appear in separate figures.

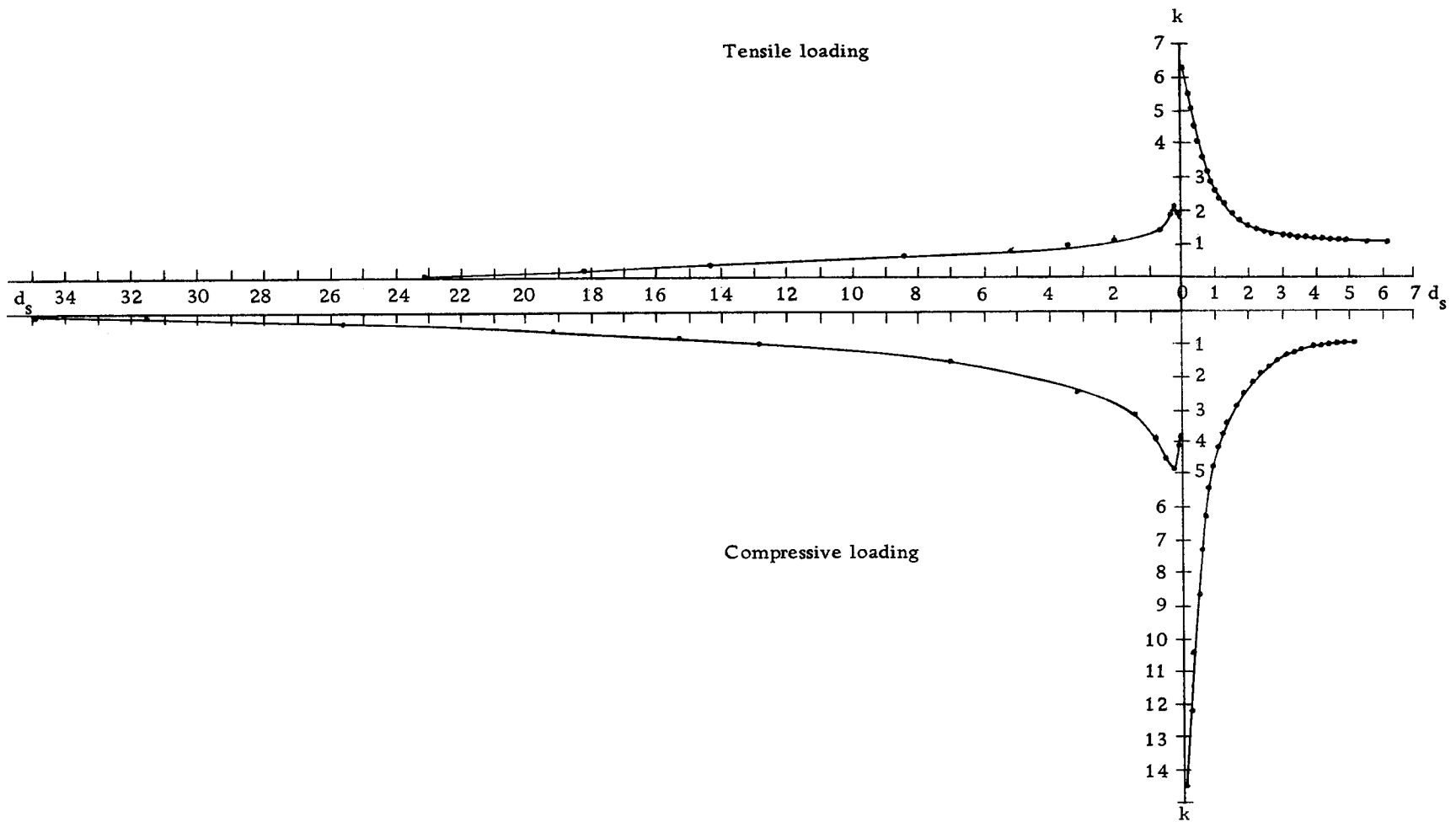


Figure 7. Square ended stiffener, longitudinal distribution of normal stress concentrations in the matrix under the tip of the stiffener and shear stress concentrations along the stiffener-matrix interface.

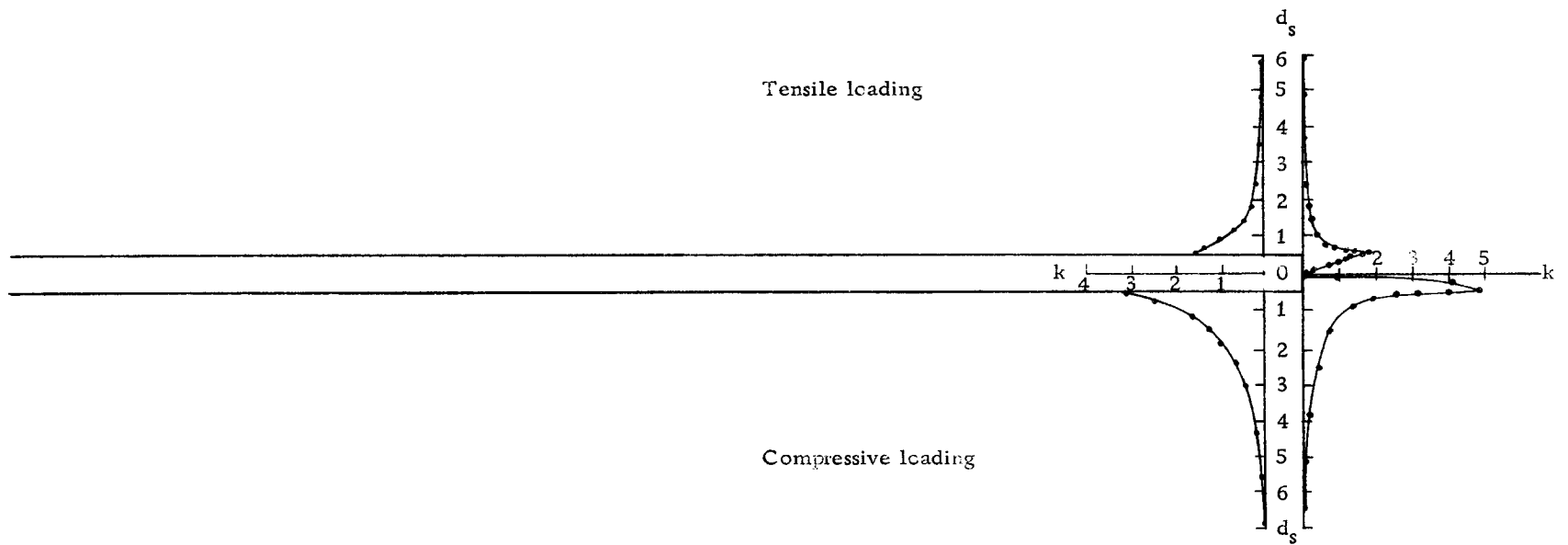


Figure 8. Square ended stiffener, radial distribution of shear stress concentrations across the region of the maximum gradient and the region of the widest range of influence.

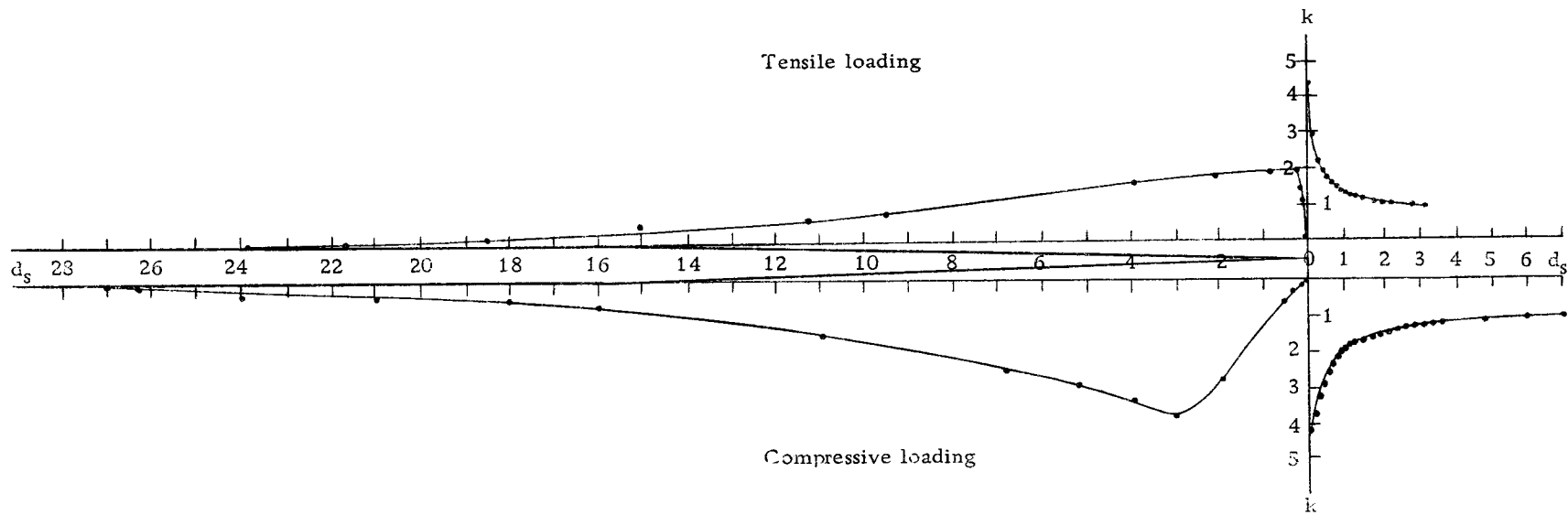


Figure 9. Tapered ended stiffener, longitudinal distribution of normal stress concentrations in the matrix under the tip of the stiffener and shear stress concentrations along the stiffener-matrix interface.

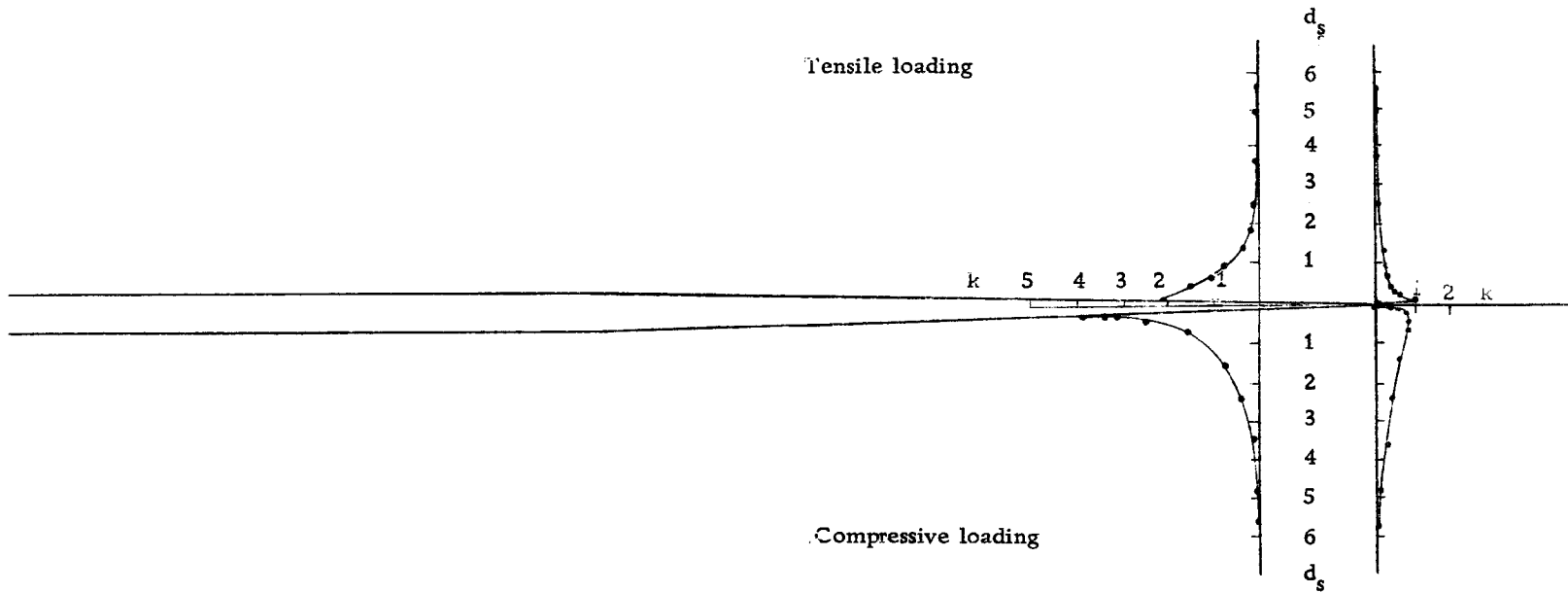


Figure 10. Tapered ended stiffener, radial distribution of shear stress concentrations across the region of the maximum gradient and the region of the widest range of influence.

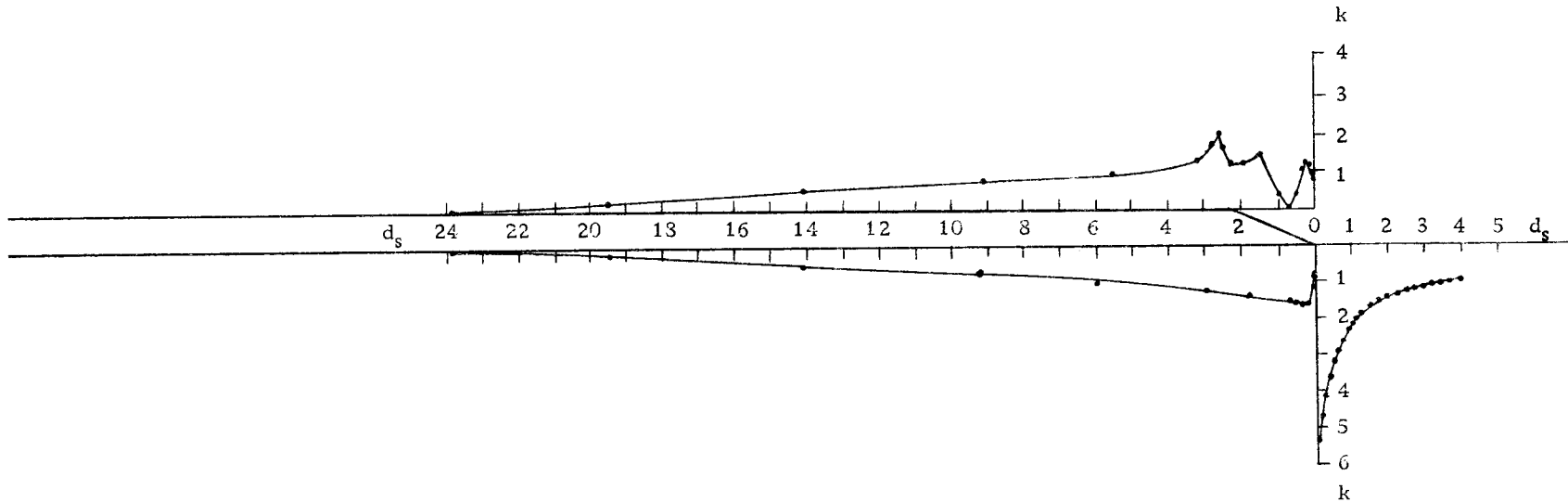


Figure 11. 18° ended stiffener, tensile loading, longitudinal distribution of normal stress concentrations in the matrix under the tip of the stiffener and shear stress concentrations along each side of the stiffener-matrix interface.

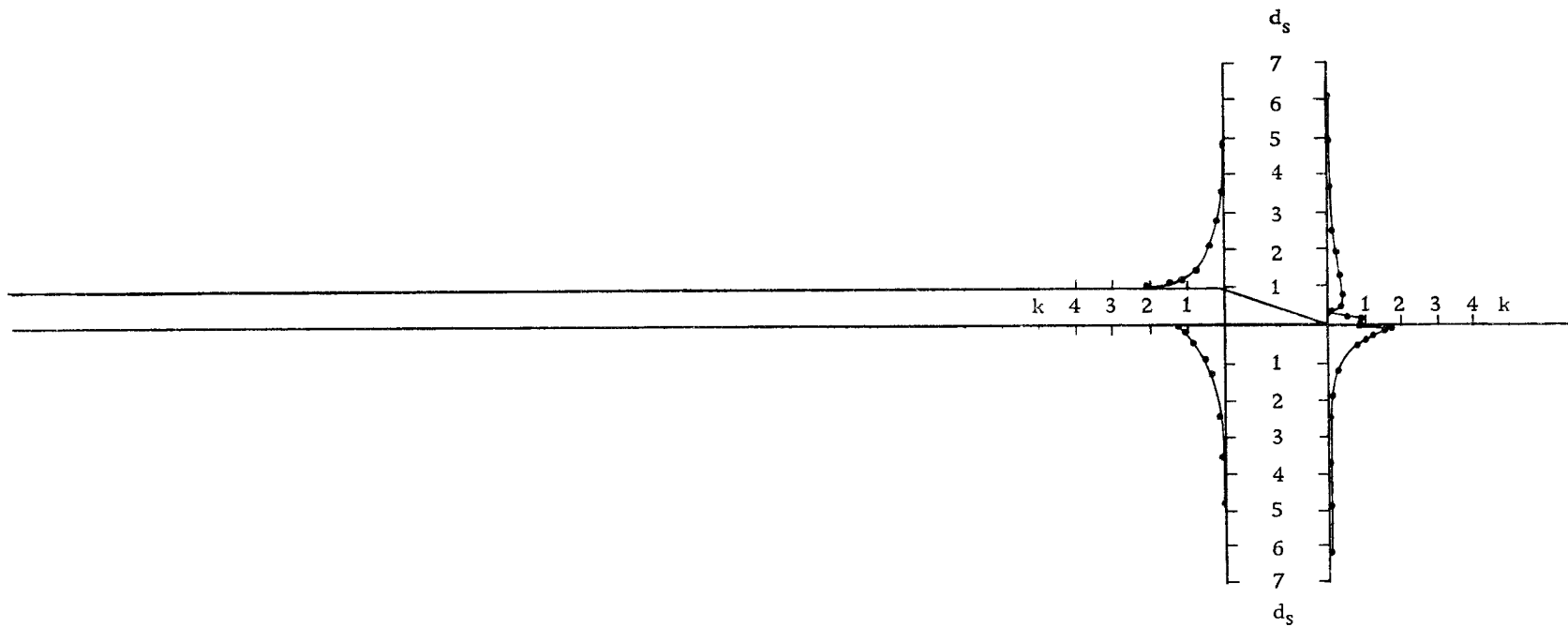


Figure 12. 18° ended stiffener, tensile loading, radial distribution of shear stress concentrations across the region of the maximum gradient and the region of the widest range of influence.

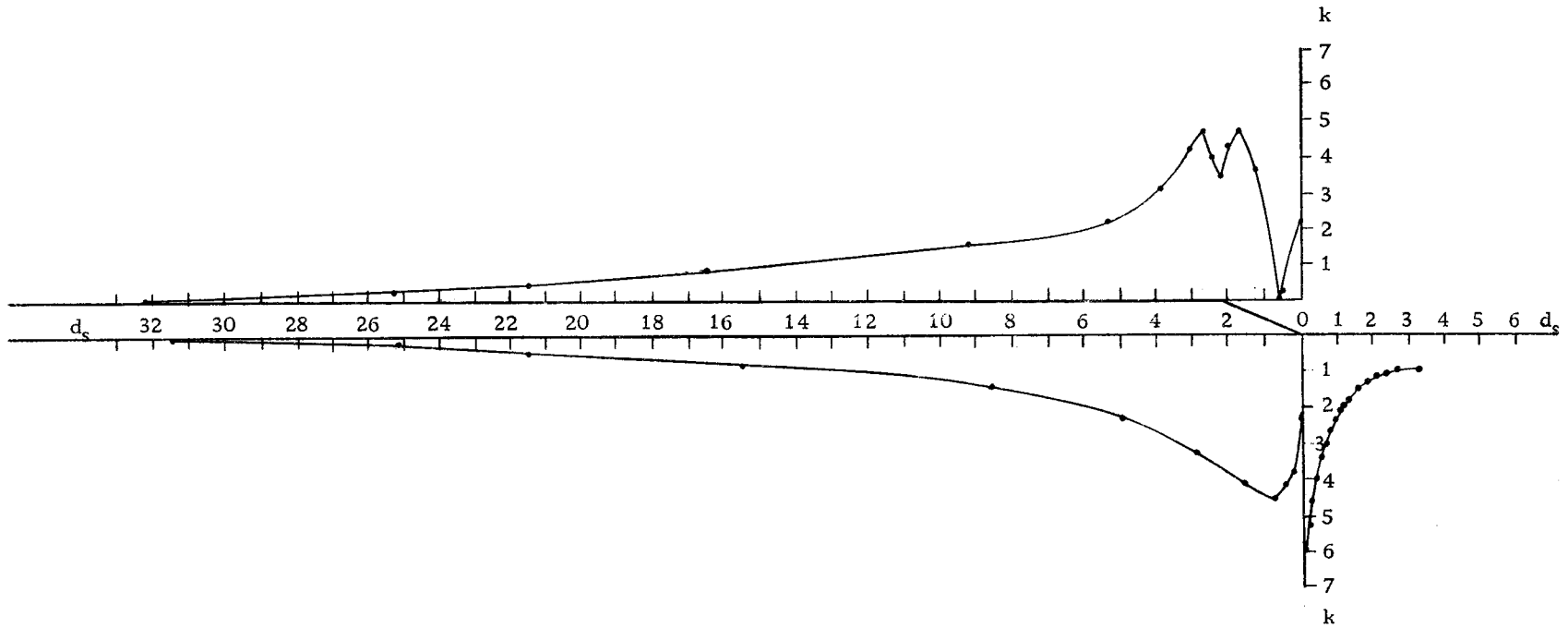


Figure 13. 18° ended stiffener, compressive loading, longitudinal distribution of normal stress concentrations in the matrix under the tip of the stiffener and shear stress concentrations along each side of the stiffener-matrix interface.

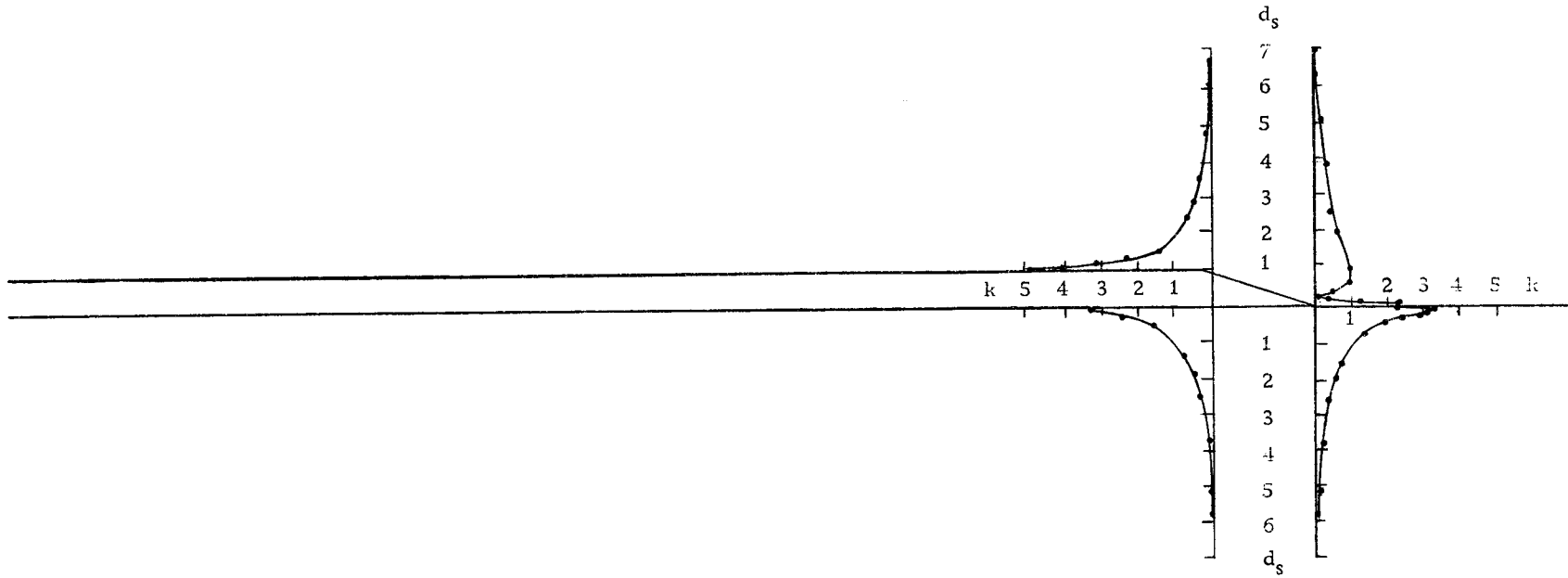


Figure 14. 18° ended stiffener, compressive loading, radial distribution of shear stress concentrations across the region of the maximum gradient and the region of the widest range of influence.

BIBLIOGRAPHY

1. Bonem, Frank. Silicon carbide whiskers, metallic filaments hurdle economic barrier. *Research/Development* 16:24-25. March, 1965.
2. Carborundum Company, Inorganic fibrous materials, silicon carbide whisker filaments. Niagara Falls, New York, n. d. 1 sheet (Bulletin no. 202)
3. Compton, K. G., A. Mendizza and S. M. Arnold. Filamentary growths on metal surfaces. *Corrosion* 7:327-334. 1951.
4. Cottrell, A. H. Strong solids. *Proceedings of the Royal Society of London, Ser. A*, 282:2-9. 1964.
5. Cox, H. L. The elasticity and strength of paper and other fibrous materials. *British Journal of Applied Physics* 3:72-79. 1952.
6. Cratchley, D. Experimental aspects of fibre-reinforced metals. *Metallurgical Reviews* 10:79-144. 1965.
7. Dana, Edward S. Dana's manual of mineralogy. 15th ed. New York, John Wiley, 1941. 480 p.
8. Daniel, I. M. and A. J. Durelli. Shrinkage stresses around rigid inclusions. *Experimental Mechanics* 2:240-244. 1962.
9. Designing strength into materials. *Business Week*, December 17, 1966. p. 91-98.
10. Dow, Norris F. Study of stresses near a discontinuity in a filament-reinforced composite metal. Valley Forge, Pennsylvania, General Electric Company, 1963. 49 p. (R63SD61)
11. Epstein, George. Adhesive bonding of metals. New York, Reinhold, 1954. 218 p.
12. Frocht, Max M. Photoelasticity. Vol. 1. New York, John Wiley, 1941. 411 p.

13. Haslett, William H. and Frederick J. McGarry. Shrinkage stresses in glass filament-resin systems. *Modern Plastics* 40:135-192. December, 1962.
14. Herring, Conyers and J. K. Galt. Elastic and plastic properties of very small metal specimens. *Physical Review* 85:1060-1061. 1952.
15. Holliday, Leslie (ed.) *Composite materials*. New York, Elsevier, 1966. 540 p.
16. Jackson, P. W. and D. Cratchley. The effect of fibre orientation on the tensile strength of fibre-reinforced metals. *Journal of the Mechanics and Physics of Solids* 14:49-64. 1966.
17. Jones, Russel C. *Structural metal composites*. *Civil Engineering* 37:54-57. February, 1967.
18. Kelly, Anthony. Royal society discussion on new materials, 1963. *Proceedings of the Royal Society of London, Ser. A*, 282:63-79. 1964.
19. Kelly, Anthony. Fiber-reinforced metals. *Scientific American* 212:28-37. February, 1965.
20. Kelly, Anthony and G. J. Davies. The principles of the fibre reinforcement of metals. *Metallurgical Reviews* 10:1-79. 1965.
21. Kelly, Anthony and W. R. Tyson. Tensile properties of fibre-reinforced metals. *Journal of the Mechanics and Physics of Solids* 13:329-350. 1965.
22. Krock, Richard and Robert Kelsey. Whiskers--their promise and problems. *Industrial Research* 7:46-57. February, 1965.
23. Levitt, Albert P. Whisker strengthened metals. *Mechanical Engineering* 89:36-42. January, 1967.
24. McDanel, D. L., R. W. Jech and J. W. Weeton. Analysis of stress-strain behavior of tungsten-fiber-reinforced copper composites. *Transactions of the AIME* 233:636-642. 1965.
25. MacLaughlin, Thomas F. Effect of fiber geometry on stress in fiber-reinforced composite materials. *Experimental Mechanics* 6:481-492. 1966.

26. McQueen, Hugh. Fiber composites. *Engineering Journal* 48:30-39. November, 1965.
27. Mayer, Norman. Structural applications for advanced composite materials. *Metals Engineering Quarterly* 5:44-49. August, 1965.
28. Milewski, John V. R & D challenge of whisker composites. *Research/Development* 17:3034. March, 1966.
29. Miller, Donald G. et al. Metal reinforced ceramic composites. *Bulletin of the American Ceramic Society* 45:513-518. 1966.
30. Mindlin, R. D. A review of the photoelastic method of stress analysis II. *Journal of Applied Physics* 10:273-294. 1939.
31. National Research Council. Report of the ad-hoc committee on interface problems in fibrous composites. Washington, D. C. , 1965. (N66-24747) (Microfiche)
32. Outwater, J. Ogden. Plastics reinforcement in tension. *Modern Plastics* 33:156-248. March, 1956.
33. Outwater, J. Ogden. Composite materials. *Mechanical Engineering* 88:32-39. February, 1966.
34. Outwater, J. Ogden and D. C. West. Stress distribution in the resin of reinforced plastics. *Modern Plastics* 39:154-252. September, 1961.
35. Perry, Henry A. Adhesive bonding of reinforced plastics. New York, McGraw Hill, 1959. 275 p.
36. Petrasek, D. W. and John Weeton. Alloying effects on tungsten-fibre-reinforced copper-alloy or high-temperature-alloy matrix composites. Washington, 1963. 64 p. (U. S. National Aeronautics and Space Administration Technical Note TN D-1568)
37. Piehler, Henry R. Plastic deformation and failure of silver-steel filament composites. *Transactions of the AIME* 233:12-16. 1965.
38. Piggott, M. R. A theory of fiber strengthening. *Acta Metallurgica* 14:1429-1435. 1966.

39. Price, D. E. and H. J. Wagner. Preparation and properties of fiber-reinforced structural materials. Columbus, 1963. 21 p. (Battelle Memorial Institute. Defense Metals Information Center. DMIC memorandum 176)
40. Rosen, B. Walter. Tensile failure of fibrous composites. AIAA Journal 2:1985-1991. 1964.
41. Rosen, B. Walter, Norris F. Dow and Z. Hashin. Mechanical properties of fibrous composites. Washington, 1964. 150 p. (U. S. National Aeronautics and Space Administration. CR-31)
42. Schuster, D. M. and E. Scala. The mechanical interaction of sapphire whiskers with a birefringent matrix. Transactions of the AIME 230:1635-1640. 1964.
43. Sutton, Willard H. Development of composite structural materials for space vehicle applications. Journal of the American Rocket Society 32:593-600. 1962.
44. Sutton, Willard H., B. Walter Rosen and D. G. Flom. Whisker-reinforced plastics for space applications. Journal of the Society of Plastics Engineers 20:1203-1209. 1964.
45. Tyson, W. R. and G. J. Davies. A photoelastic study of the shear stresses associated with the transfer of stress during fibre reinforcement. British Journal of Applied Physics 16:199-205. 1965.
46. West, Phillip. Whisker composites: where do they stand today? Materials in Design Engineering 61:112-116. June, 1965.
47. Zackey, Victor F. (ed.) High strength materials. New York, John Wiley, 1965. 879 p.

APPENDIX

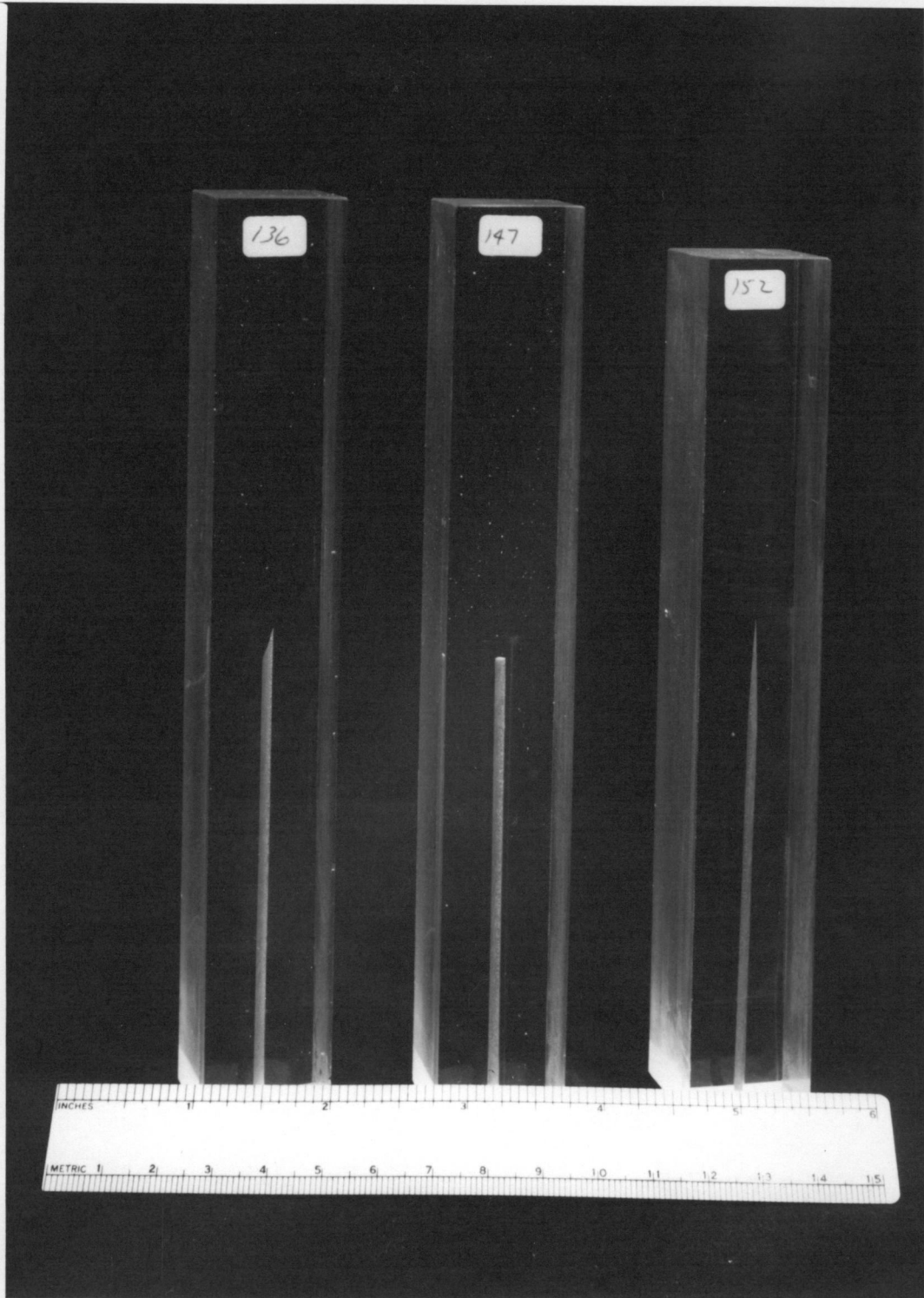


Figure 15. Typical models used in this investigation.

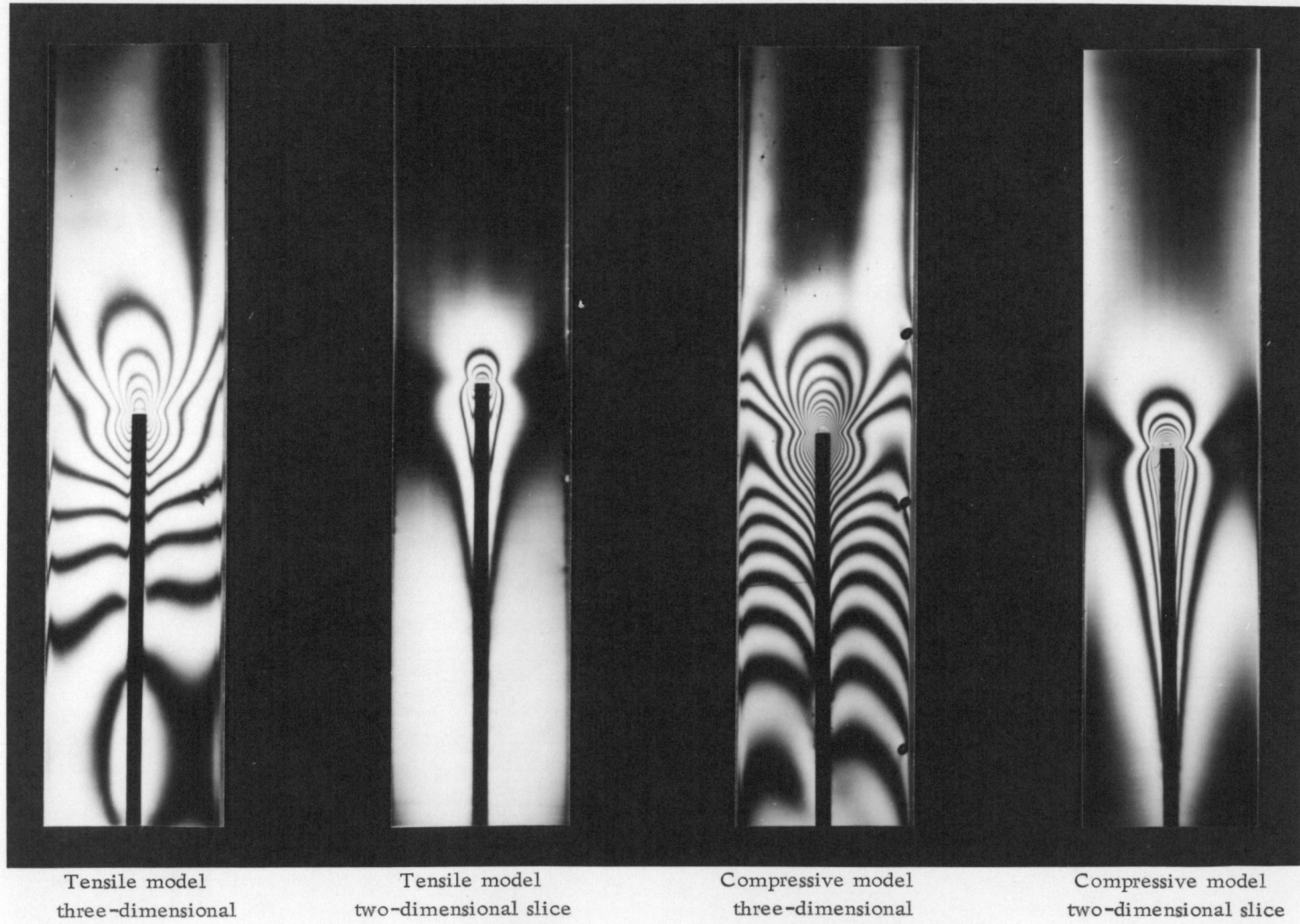
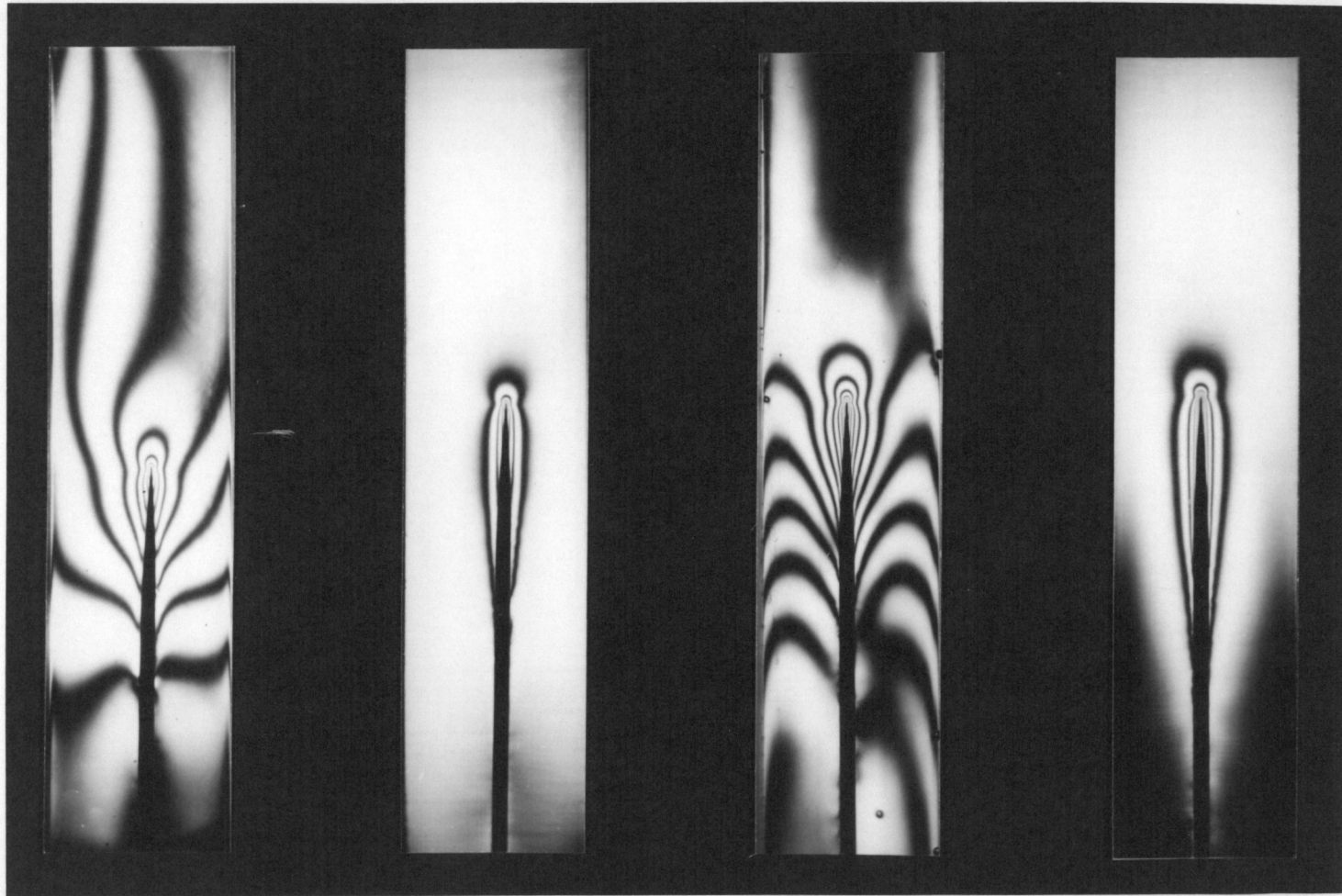


Figure 16. Models with square ended stiffeners.



Tensile model
three-dimensional

Tensile model
two-dimensional slice

Compressive model
three-dimensional

Compressive model
two-dimensional slice

Figure 17. Models with tapered ended stiffeners.

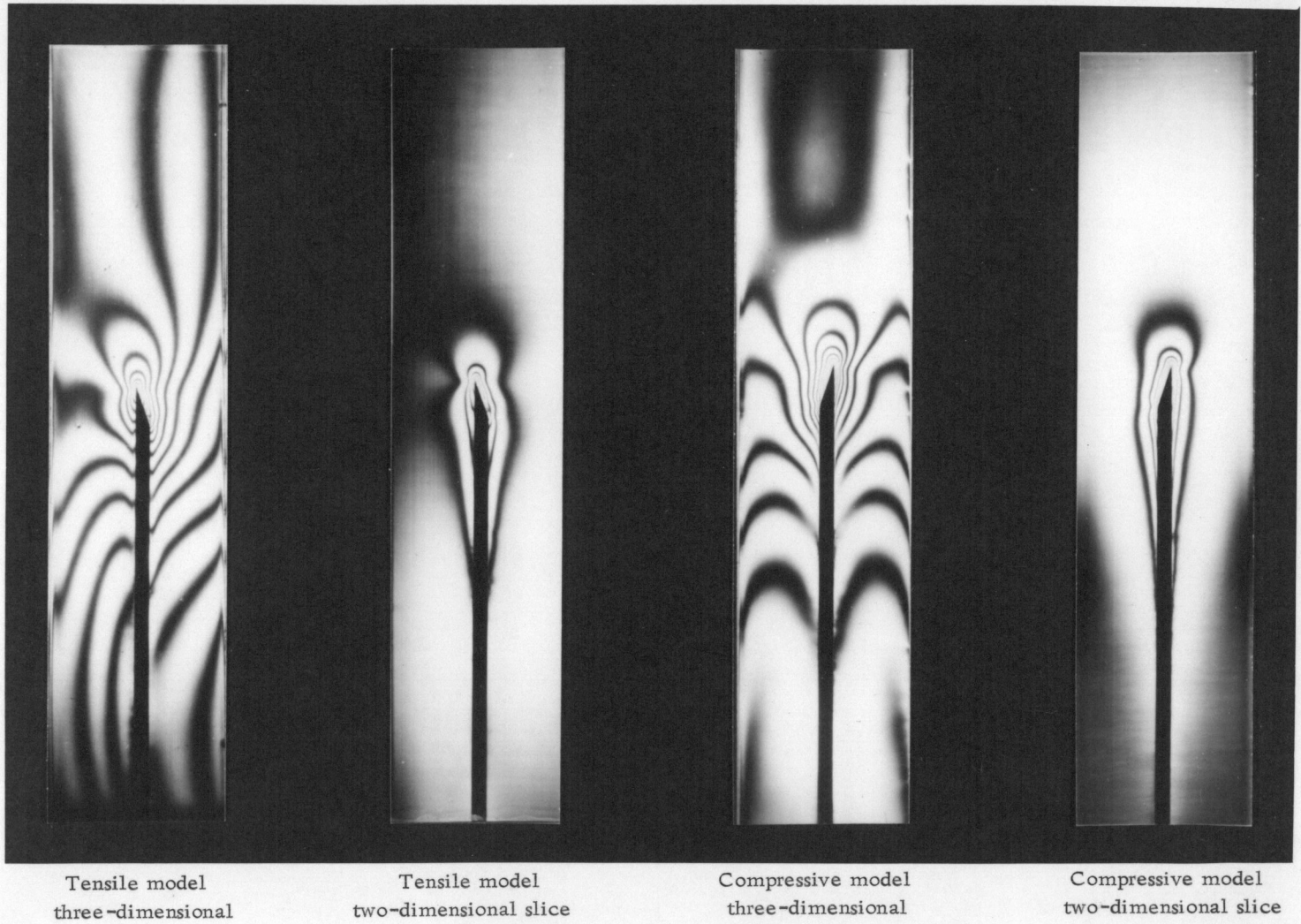
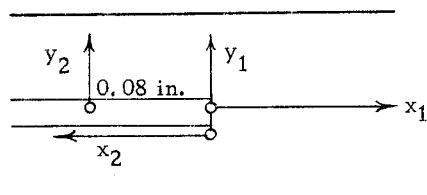


Figure 18. Models with 18° ended stiffener.

Table 1. Tension model, basal parting {0001} (square end).



$$\sigma_n = 1.08 \text{ fringe}$$

$$d_s = 0.082 \text{ in.}$$

x_1	$\frac{x_1}{d_s}$	σ	$k = \frac{\sigma}{\sigma_n}$	x_2	$\frac{x_2}{d_s}$	τ	$k = \frac{\tau}{\sigma_n}$
0.00 in.	0.00	6.81 fringe	6.3	0.000 in.	0.00	2.02 fringe	1.86
0.01	0.12	5.95	5.5	0.005	0.06	2.10	1.94
0.02	0.24	5.48	5.07	0.017	0.21	2.34	2.17
0.03	0.37	4.97	4.59	0.036	0.44	2.07	1.92
0.04	0.49	4.44	4.11	0.079	0.96	1.80	1.67
0.05	0.61	3.92	3.62	0.175	2.13	1.35	1.25
0.06	0.73	3.42	3.18	0.315	3.84	1.10	1.02
0.07	0.85	3.07	2.84	0.447	5.45	0.96	0.89
0.08	0.98	2.80	2.59	0.700	8.54	0.67	0.62
0.09	1.10	2.55	2.36	1.180	14.40	0.39	0.36
0.10	1.22	2.36	2.18	1.500	18.30	0.22	0.20
0.12	1.46	2.06	1.91	1.890	23.05	0.00	0.00
0.14	1.71	1.84	1.70				
0.16	1.95	1.66	1.54				
0.18	2.20	1.52	1.41				
0.20	2.44	1.42	1.32				
0.22	2.68	1.38	1.28				
0.24	2.93	1.35	1.25				
0.26	3.17	1.32	1.22				
0.28	3.41	1.29	1.19				
0.30	3.66	1.26	1.17				
0.32	3.90	1.24	1.15				
0.34	4.15	1.22	1.13				
0.36	4.39	1.20	1.11				
0.38	4.63	1.19	1.10				
0.40	4.88	1.18	1.09				
0.45	5.50	1.13	1.05				
0.50	6.10	1.08	1.00				
∞	∞	1.08	1.00				

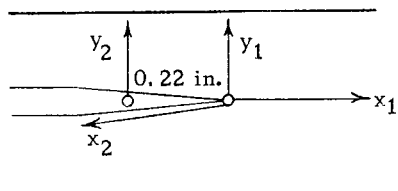
Table 1. Continued.

y_1	$\frac{y_1}{d_s}$	τ	$k = \frac{\tau}{\sigma_n}$	y_2	$\frac{y_2}{d_s}$	τ	$k = \frac{\tau}{\sigma_n}$
0.000 in.	0.00	0.00 fringe	0.00	0.000 in.	0.00	---	---
0.007	0.09	0.31	0.28	0.041	0.50	1.78 fringe	1.65
0.017	0.21	0.75	0.69	0.061	0.73	1.50	1.39
0.025	0.31	1.06	0.98	0.075	0.91	1.18	1.09
0.030	0.37	1.25	1.16	0.095	1.12	0.86	0.80
0.035	0.43	1.50	1.39	0.115	1.36	0.56	0.52
0.038	0.46	1.75	1.62	0.160	1.89	0.32	0.30
0.041	0.50	1.96	1.81	0.200	2.44	0.18	0.17
0.043	0.53	1.50	1.39	0.300	3.66	0.04	0.04
0.046	0.56	1.25	1.16	0.400	4.88	0.00	0.00
0.051	0.62	0.91	0.84	0.480	5.92	0.00	0.00
0.063	0.77	0.63	0.58				
0.085	1.09	0.41	0.38				
0.120	1.46	0.23	0.21				
0.150	1.83	0.19	0.18				
0.200	2.44	0.08	0.07				
0.300	3.66	0.00	0.00				
0.400	4.88	0.00	0.00				
0.485	5.92	0.00	0.00				

Table 2. Continued.

y_1	$\frac{y_1}{d_s}$	τ	$k = \frac{\tau}{\sigma_n}$	y_2	$\frac{y_2}{d_s}$	τ	$k = \frac{\tau}{\sigma_n}$
0.00 in.	0.00	0.00 fringe	0.00	0.000 in.	0.00	---	---
0.004	0.05	0.60	0.94	0.039	0.50	1.99 fringe	3.11
0.013	0.17	2.60	4.07	0.064	0.82	1.62	2.53
0.035	0.45	3.03	4.73	0.089	1.19	1.05	1.64
0.039	0.50	2.49	3.90	0.114	1.46	0.82	1.28
0.042	0.53	1.98	3.10	0.139	1.78	0.63	0.99
0.044	0.56	1.58	2.49	0.189	2.42	0.42	0.66
0.049	0.63	1.21	1.89	0.239	3.06	0.25	0.39
0.065	0.83	0.85	1.33	0.339	4.35	0.10	0.16
0.122	1.57	0.43	0.66	0.439	5.62	0.04	0.06
0.200	2.56	0.23	0.36	0.514	6.58	0.00	0.00
0.300	3.85	0.11	0.17				
0.400	5.13	0.04	0.06				
0.500	6.42	0.00	0.00				

Table 3. Tension model (tapered end).

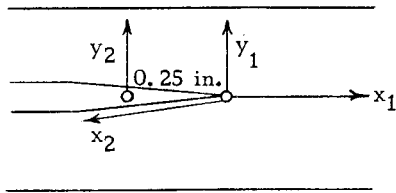


$\sigma_n = 0.69$ fringe
 $d_s = 0.081$ in.

x_1	$\frac{x_1}{d_s}$	σ	$k = \frac{\sigma}{\sigma_n}$	x_2	$\frac{x_2}{d_s}$	τ	$k = \frac{\tau}{\sigma_n}$
0.00 in.	0.00	3.01 fringe	4.37	0.000 in.	0.00	0.00 fringe	0.00
0.01	0.12	2.03	2.95	0.010	0.12	0.73	1.06
0.02	0.25	1.51	2.19	0.020	0.25	0.95	1.38
0.03	0.37	1.30	1.88	0.036	0.44	1.39	2.02
0.04	0.49	1.17	1.70	0.091	1.02	1.37	1.99
0.05	0.62	1.09	1.58	0.172	2.12	1.34	1.94
0.06	0.74	1.02	1.48	0.316	3.90	1.12	1.62
0.07	0.86	0.95	1.38	0.488	6.02	0.95	1.38
0.08	0.99	0.89	1.29	0.777	9.60	0.66	0.96
0.09	1.11	0.84	1.22	1.085	13.40	0.50	0.72
0.10	1.23	0.80	1.16	1.25	15.44	0.37	0.54
0.12	1.48	0.77	1.12	1.5	18.52	0.19	0.28
0.14	1.73	0.75	1.09	1.75	21.60	0.09	0.13
0.16	1.98	0.73	1.06	1.925	23.80	0.00	0.00
0.18	2.22	0.72	1.04				
0.22	2.72	0.71	1.03				
0.26	3.21	0.69	1.00				
∞	∞	0.69	1.00				

y_1	$\frac{y_1}{d_s}$	τ	$k = \frac{\tau}{\sigma_n}$	y_2	$\frac{y_2}{d_s}$	τ	$k = \frac{\tau}{\sigma_n}$
0.00 in.	0.00	0.00 fringe	0.00	0.000 in.	0.00	---	---
0.006	0.07	0.69	1.00	0.023	0.28	1.47 fringe	2.13
0.010	0.12	0.42	0.61	0.036	0.45	1.15	1.67
0.014	0.17	0.36	0.52	0.049	0.61	0.72	1.04
0.019	0.23	0.30	0.43	0.079	0.97	0.57	0.83
0.025	0.31	0.24	0.35	0.110	1.36	0.25	0.36
0.049	0.61	0.22	0.32	0.150	1.85	0.18	0.26
0.067	0.83	0.19	0.28	0.200	2.47	0.08	0.12
0.100	1.23	0.14	0.20	0.300	3.71	0.04	0.06
0.200	2.47	0.05	0.07	0.400	4.94	0.01	0.01
0.300	3.71	0.01	0.02	0.450	5.56	0.00	0.00
0.400	4.94	0.01	0.01				
0.450	5.56	0.00	0.00				

Table 4. Compression model (tapered end).

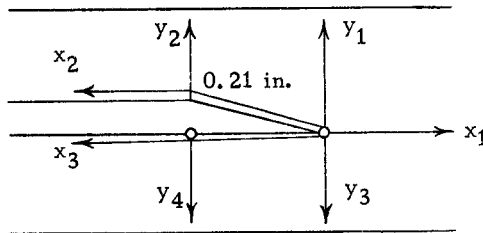


$$\sigma_n = 0.56 \text{ fringe}$$

$$d_s = 0.083 \text{ in.}$$

x_1	$\frac{x_1}{d_s}$	σ	$k = \frac{\sigma}{\sigma_n}$	x_2	$\frac{x_2}{d_s}$	τ	$k = \frac{\tau}{\sigma_n}$
0.00 in.	0.00	2.36 fringe	4.22	0.000 in.	0.00	0.00 fringe	0.00
0.01	0.12	2.08	3.72	0.007	0.08	0.05	0.09
0.02	0.24	1.83	3.27	0.031	0.37	0.10	0.18
0.03	0.36	1.62	2.90	0.048	0.58	0.30	0.54
0.04	0.48	1.46	2.61	0.144	1.74	1.63	2.91
0.05	0.60	1.31	2.34	0.250	3.01	2.22	3.96
0.06	0.72	1.21	2.16	0.315	3.80	1.94	3.47
0.07	0.84	1.12	2.00	0.450	5.42	1.75	3.12
0.08	0.96	1.06	1.89	0.60	7.22	1.50	2.68
0.09	1.08	1.02	1.82	0.925	11.13	0.94	1.68
0.10	1.20	0.99	1.77	1.350	16.25	0.38	0.68
0.12	1.45	0.96	1.71	1.500	18.09	0.29	0.52
0.14	1.69	0.91	1.63	1.750	21.08	0.16	0.29
0.16	1.93	0.87	1.55	2.000	24.10	0.08	0.14
0.18	2.17	0.83	1.48	2.250	27.10	0.00	0.00
0.20	2.41	0.79	1.41				
0.22	2.65	0.76	1.36				
0.24	2.89	0.74	1.32				
0.26	3.13	0.72	1.29				
0.28	3.37	0.71	1.27				
0.30	3.61	0.70	1.25				
0.40	4.82	0.65	1.16				
0.50	6.03	0.60	1.07				
0.60	7.23	0.58	1.04				
∞	∞	0.56	1.00				

y_1	$\frac{y_1}{d_s}$	τ	$k = \frac{\tau}{\sigma_n}$	y_2	$\frac{y_2}{d_s}$	τ	$k = \frac{\tau}{\sigma_n}$
0.00 in.	0.00	0.00 fringe	0.00	0.000 in.	0.00	---	---
0.005	0.06	0.17	0.30	0.018	0.22	2.22 fringe	3.96
0.009	0.11	0.28	0.50	0.022	0.27	1.94	3.46
0.016	0.19	0.41	0.73	0.025	0.30	1.85	3.30
0.035	0.42	0.41	0.73	0.040	0.48	1.44	2.57
0.050	0.60	0.41	0.73	0.068	0.82	0.95	1.70
0.112	1.35	0.31	0.55	0.143	1.72	0.43	0.77
0.200	2.41	0.19	0.34	0.200	2.41	0.30	0.53
0.300	3.62	0.12	0.21	0.300	3.62	0.13	0.23
0.400	4.82	0.04	0.07	0.400	4.82	0.04	0.07
0.475	5.72	0.00	0.00	0.475	5.72	0.00	0.00

Table 5. Tension model, rhombohedral parting $\{10 \bar{1} 1\}$ (18° end).

$$\sigma_n = 0.89 \text{ fringe}$$

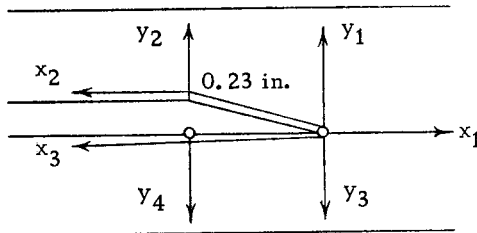
$$d_s = 0.082 \text{ in.}$$

x_1	$\frac{x_1}{d_s}$	σ	$k = \frac{\sigma}{\sigma_n}$	x_2	$\frac{x_2}{d_s}$	τ	$k = \frac{\tau}{\sigma_n}$
0.00 in.	0.00	4.76 fringe	5.35	0.000 in.	0.00	-0.73 fringe	-0.82
0.01	0.12	4.18	4.70	0.002	0.02	-0.77	-0.86
0.02	0.24	3.70	4.16	0.009	0.11	-1.03	-1.16
0.03	0.37	3.22	3.62	0.015	0.18	-1.07	-1.20
0.04	0.49	2.85	3.20	0.025	0.30	-1.01	-1.04
0.05	0.61	2.57	2.89	0.050	0.61	-0.31	-0.35
0.06	0.73	2.34	2.63	0.060	0.73	0.00	0.00
0.07	0.85	2.06	2.32	0.081	0.99	0.31	0.35
0.08	0.98	1.91	2.14	0.138	1.68	1.44	1.62
0.09	1.10	1.77	1.99	0.162	1.98	1.15	1.30
0.10	1.22	1.66	1.87	0.184	2.22	1.15	1.30
0.12	1.46	1.47	1.65	0.194	2.36	1.65	1.85
0.14	1.71	1.36	1.53	0.212	2.59	1.90	2.14
0.14	1.95	1.24	1.39	0.225	2.74	1.73	1.95
0.18	2.20	1.17	1.32	0.262	3.20	1.32	1.48
0.20	2.44	1.11	1.25	0.470	5.73	0.90	1.01
0.22	2.69	1.06	1.19	0.750	9.15	0.66	0.74
0.24	2.93	1.02	1.15	1.150	14.03	0.50	0.56
0.26	3.17	0.98	1.10	1.600	19.52	0.20	0.22
0.28	3.42	0.95	1.07	1.950	23.80	0.00	0.00
0.30	3.66	0.91	1.02				
0.32	3.91	0.89	1.00				
∞	∞	0.89	1.00				
x_3	$\frac{x_3}{d_s}$	τ	$k = \frac{\tau}{\sigma_n}$				
0.000 in.	0.00	-0.75 fringe	-0.84				
0.004	0.05	-1.02	-1.15				
0.013	0.16	-1.50	-1.69				
0.026	0.32	-1.50	-1.69				
0.040	0.49	-1.47	-1.65				
0.064	0.78	-1.39	-1.56				
0.162	1.98	-1.41	-1.58				
0.247	2.96	-1.08	-1.21				
0.487	5.95	-0.90	-1.01				
0.750	9.15	-0.65	-0.73				
1.150	14.03	-0.50	-0.56				
1.600	19.52	-0.20	-0.23				
1.950	23.80	0.00	0.00				

Table 5. Continued.

y_1	$\frac{y_1}{d_s}$	τ	$k = \frac{\tau}{\sigma_n}$	y_2	$\frac{y_2}{d_s}$	τ	$k = \frac{\tau}{\sigma_n}$
0.000 in.	0.00	-0.71 fringe	-0.80	0.000 in.	0.00	---	---
0.006	0.07	-0.73	-0.82	0.081	1.00	1.82 fringe	2.05
0.012	0.15	-0.43	-0.48	0.088	1.07	1.39	1.56
0.018	0.22	0.00	0.00	0.095	1.16	1.11	1.25
0.021	0.27	0.03	0.03	0.118	1.44	0.67	0.75
0.034	0.42	0.27	0.30	0.167	2.04	0.40	0.45
0.060	0.73	0.34	0.38	0.228	2.78	0.15	0.17
0.105	1.28	0.26	0.29	0.300	3.66	0.02	0.02
0.153	1.87	0.19	0.21	0.400	4.88	0.00	0.00
0.200	2.44	0.09	0.10	0.500	6.10	0.00	0.00
0.300	3.66	0.03	0.03				
0.400	4.88	0.00	0.00				
0.500	6.10	0.00	0.00				

y_3	$\frac{y_3}{d_s}$	τ	$k = \frac{\tau}{\sigma_n}$	y_4	$\frac{y_4}{d_s}$	τ	$k = \frac{\tau}{\sigma_n}$
0.000 in.	0.00	-0.71 fringe	-0.80	0.000 in.	0.00	1.14 fringe	1.28
0.0004	0.05	-1.50	-1.69	0.008	0.10	1.05	1.18
0.007	0.09	-1.32	-1.44	0.038	0.46	0.79	0.89
0.012	0.15	-1.06	-1.19	0.075	0.91	0.50	0.56
0.020	0.24	-0.88	-0.99	0.100	1.22	0.33	0.37
0.035	0.43	-0.62	-0.70	0.200	2.44	0.13	0.15
0.100	1.22	-0.17	-0.19	0.300	3.66	0.07	0.08
0.150	1.83	-0.08	-0.09	0.400	4.88	0.00	0.00
0.200	2.44	-0.02	-0.02	0.475	5.80	0.00	0.00
0.300	3.66	0.00	0.00				
0.400	4.88	0.00	0.00				
0.500	6.10	0.00	0.00				

Table 6. Compression model, rhombohedral parting $\{10\bar{1}1\}$ (18° end).

$$\sigma_n = 0.61 \text{ fringe}$$

$$d_s = 0.079 \text{ in.}$$

x_1	$\frac{x_1}{d_s}$	σ	$k = \frac{\sigma}{\sigma_n}$	x_2	$\frac{x_2}{d_s}$	τ	$k = \frac{\tau}{\sigma_n}$
0.00 in.	0.00	3.62 fringe	5.92	0.000 in.	0.00	-1.37 fringe	-2.24
0.01	0.13	3.17	5.20	0.050	0.63	-0.14	-0.23
0.02	0.25	2.74	4.50	0.055	0.70	0.00	0.00
0.03	0.38	2.36	3.89	0.100	1.26	2.35	3.86
0.04	0.51	2.04	3.35	0.150	1.90	2.90	4.75
0.05	0.63	1.79	2.93	0.172	2.18	2.65	4.35
0.06	0.76	1.56	2.57	0.188	2.38	2.25	3.69
0.07	0.89	1.39	2.27	0.211	2.67	2.46	4.03
0.08	1.01	1.25	2.04	0.234	2.96	2.95	4.83
0.09	1.14	1.14	1.87	0.262	3.32	2.50	4.10
0.10	1.26	1.04	1.70	0.316	4.00	1.97	3.23
0.12	1.52	0.87	1.43	0.437	5.52	1.46	2.39
0.14	1.77	0.78	1.28	0.720	9.10	0.95	1.56
0.16	2.02	0.70	1.14	1.30	16.45	0.47	0.77
0.18	2.28	0.65	1.07	1.70	21.50	0.24	0.39
0.20	2.53	0.63	1.02	2.00	25.30	0.15	0.25
0.25	3.16	0.61	1.00	2.50	31.60	0.00	0.00
0.30	3.80	0.61	1.00				
0.35	4.43	0.61	1.00				
∞	∞	0.61	1.00				

x_3	$\frac{x_3}{d_s}$	τ	$k = \frac{\tau}{\sigma_n}$
0.000 in.	0.00	-1.37 fringe	-2.24
0.025	0.32	-2.35	-3.85
0.044	0.56	-2.52	-4.12
0.074	0.94	-2.82	-4.62
0.136	1.72	-2.48	-4.07
0.235	2.97	-2.00	-3.28
0.400	5.07	-1.45	-2.38
0.675	8.53	-0.90	-1.48
1.225	15.50	-0.45	-0.74
1.700	21.50	-0.23	-0.38
2.000	25.30	-0.11	-0.18
2.450	31.00	-0.00	-0.00

Table 6. Continued.

y_1	$\frac{y_1}{d_s}$	τ	$k = \frac{\tau}{\sigma_n}$	y_2	$\frac{y_2}{d_s}$	τ	$k = \frac{\tau}{\sigma_n}$
0.000 in.	0.00	-1.37 fringe	-2.24	0.000 in.	0.00	---	---
0.006	0.08	-0.79	-1.29	0.079	1.00	2.98 fringe	4.88
0.012	0.15	-0.21	-0.34	0.086	1.09	2.47	4.05
0.019	0.24	0.09	0.15	0.092	1.16	1.97	3.23
0.027	0.34	0.28	0.46	0.101	1.28	1.47	2.41
0.045	0.57	0.56	0.92	0.123	1.55	0.95	1.55
0.079	1.00	0.56	0.92	0.194	2.45	0.45	0.74
0.162	2.05	0.35	0.57	0.229	2.90	0.35	0.57
0.250	2.53	0.25	0.41	0.279	3.53	0.23	0.38
0.300	3.79	0.18	0.30	0.379	4.80	0.09	0.15
0.400	5.07	0.08	0.13	0.479	6.05	0.02	0.03
0.500	6.32	0.02	0.03	0.529	6.70	0.00	0.00
0.550	6.95	0.00	0.00				
y_3	$\frac{y_3}{d_s}$	τ	$k = \frac{\tau}{\sigma_n}$	y_4	$\frac{y_4}{d_s}$	τ	$k = \frac{\tau}{\sigma_n}$
0.000 in.	0.00	-1.37 fringe	-2.24	0.000 in.	0.00	2.00 fringe	3.28
0.006	0.08	-1.96	-3.21	0.018	0.23	1.50	2.46
0.012	0.15	-1.85	-3.03	0.046	0.58	1.00	1.64
0.016	0.20	-1.74	-2.85	0.117	1.48	0.48	0.79
0.021	0.27	-1.44	-2.36	0.150	1.90	0.36	0.59
0.031	0.39	-1.15	-1.89	0.200	2.53	0.22	0.36
0.054	0.68	-0.83	-1.36	0.300	3.79	0.07	0.11
0.116	1.47	-0.45	-0.74	0.400	5.07	0.01	0.02
0.150	1.70	-0.34	-0.56	0.450	5.70	0.00	0.00
0.200	2.53	-0.21	-0.34				
0.300	3.79	-0.10	-0.16				
0.400	5.07	-0.05	-0.08				
0.450	5.70	0.00	0.00				